

PACIFIC EARTHQUAKE ENGINEERING RESEARCH CENTER

Fluid-Structure Interaction and Python-Scripting Capabilities in OpenSees

Minjie Zhu

Michael H. Scott

School of Civil and Construction Engineering
Oregon State University

PEER Report No. 2019/06
Pacific Earthquake Engineering Research Center
Headquarters at the University of California, Berkeley

August 2019

Disclaimer

The opinions, findings, and conclusions or recommendations expressed in this publication are those of the author(s) and do not necessarily reflect the views of the study sponsor(s), the Pacific Earthquake Engineering Research Center, or the Regents of the University of California.

Fluid-Structure Interaction and Python-Scripting Capabilities in OpenSees

Minjie Zhu

Michael H. Scott

School of Civil and Construction Engineering
Oregon State University

PEER Report No. 2019/06

Pacific Earthquake Engineering Research Center
Headquarters at the University of California, Berkeley
August 2019

ABSTRACT

Building upon recent advances in OpenSees, the goals of this project are to expand the framework's Python scripting capabilities and to further develop its fluid–structure interaction (FSI) simulation capabilities, which are based on the particle finite-element method (PFEM). At its inception, the FSI modules in OpenSees were based on Python scripting. To accomplish FSI simulations in OpenSees, Python commands have been added for a limited number of pre-existing element and material commands, e.g., linear-elastic triangle elements and beam–column elements with *Concrete01/Steel01* fiber sections. Incorporation of hundreds of constitutive models and element formulations under the Python umbrella for FSI and general OpenSees use remain to be done. Although the original scripting language, *Tcl*, in OpenSees is string based, powerful, and easy to learn, it is not suitable for mathematical computations. Recent trends in scripting languages for engineering applications have embraced more general, scientific languages such as Python, which has evolved to a large community with numerous libraries for numerical computing, data analysis, scientific visualization, and web development. These libraries can be utilized with the FSI simulation for tsunami analysis. Extending OpenSees to Python will help OpenSees keep pace with new scripting developments from the scientific computing community and make the framework more accessible to graduate students, who likely have learned Python as undergraduates.

ACKNOWLEDGMENTS

This work was supported through the Transportation Systems Research Program of the Pacific Earthquake Engineering Research Center (PEER). Any opinions, findings, and conclusions or recommendations expressed in this material are those of the authors and do not necessarily reflect those of PEER or the Regents of the University of California.

TABLE OF CONTENTS

ABSTRACT	iii
ACKNOWLEDGMENTS	v
TABLE OF CONTENTS	viii
LIST OF TABLES	x
LIST OF FIGURES	xiii
1 Introduction	1
2 Fluid-Structure Interaction	3
2.1 Governing Equations	4
2.2 Finite Element Discretization	5
2.2.1 Structural equations	5
2.2.2 Fluid equations	6
2.2.3 Monolithic system	6
2.3 Time-Domain Discretization	7
2.4 Nonlinear Solution Algorithm	8
2.5 Various Solvers for FSI in OpenSees	10
2.5.1 Incompressible fractional step solver	10
2.5.2 Unified fractional step solver	11
2.6 Domain Meshing for FSI	12
2.6.1 Moving mesh method	12
2.6.2 Background mesh sethod	14
3 Implementation of FSI in OpenSees	19
3.1 Domain Meshing	19
3.2 FSM Solvers	22
3.3 Examples	22
3.3.1 Moving mesh model of a dam break as an elastic obstacle	22
3.3.2 Dam-break problem as a nonlinear material obstacle	25
3.3.3 A 2D sloshing example with unified FSM	26
4 Python Scripting in OpenSees	35
4.1 Implementation of Python Interpreter	35
4.2 Illustrative Examples	39
4.2.1 Nonlinear truss example	39

4.2.2 Dam-break problem as a nonlinear material obstacle example	41
4.3 Python Commands Manual	44
4.4 Python and <i>Tcl</i> Tests	44
5 CONCLUSIONS	53
5.1 Summary and Conclusions	53
5.2 Future Work	53
REFERENCES	55

LIST OF TABLES

3.1	Iterations to achieve convergence for different viscosity with $\Delta t = 10^{-3}$ sec.	28
3.2	Iterations to achieve convergence for different viscosity with $\Delta t = 5 \times 10^{-5}$ sec.	31
3.3	Iterations to achieve convergence for different viscosity with $\Delta t = 4 \times 10^{-6}$ sec.	33
4.1	Timing of Python and <i>Tcl</i> scripts for same models.	44
4.2	Verification of elastic SDOF systems of Python and <i>Tcl</i> with Chopra (2007) (Section 3.1).	47
4.3	Verification of elastic SDOF systems of Python and <i>Tcl</i> with Chopra (2007) (Section 6.4).	47
4.4	Verification of period for 2D Elastic Frame with SAP2000 and SeismoStruc.	47
4.5	Verification of displacement for 2D Elastic Frame with SAP2000 and SeismoStruc.	48
4.6	Prismatic beam benchmark problems with Kaehler et al. (2011) (tip displacements).	48
4.7	Prismatic beam benchmark problems with (Kaehler et al. 2011) (base moments).	49
4.8	Verification of eigenvalues of elastic frame with Bathe and Wilson (1972), SAP2000, and SeismoStruct.	49
4.9	Verification of linear elastic planar shear wall with ETABS and SAP2000.	50
4.10	Verification of shell elements with exact solutions.	50

LIST OF FIGURES

2.1	The MINI element.	6
2.2	A cloud of FSI particles.	13
2.3	Delaunay Triangulation of the cloud of FSI particles.	13
2.4	Moving mesh of the cloud of FSI particles.	14
2.5	A cloud of fluid particles.	15
2.6	The fixed-fluid mesh based on the fluid particles.	15
2.7	The fixed-fluid mesh with structure.	16
2.8	The Delaunay Triangulation between fixed fluid mesh and structure.	16
2.9	The background mesh with fixed fluid mesh and structure.	17
3.1	Class diagram of the FSI implementation in OpenSees framework.	20
3.2	<code>class Mesh</code> in OpenSees framework.	20
3.3	FSM solvers in OpenSees framework.	21
3.4	Elastic obstacle with moving mesh.	23
3.5	Snapshots of dam break as an elastic obstacle with moving mesh.	23
3.6	Snapshots of dam break as an elastic obstacle with background mesh.	24
3.7	Comparison of the displacements of the free end of the elastic obstacle with different numerical approaches.	24
3.8	Nonlinear material for obstacle in dam-break problem and comparison of free-end displacements with elastic material.	25
3.9	Model of 2D water sloshing analysis in a rectangular tank.	26
3.10	Snapshots of water sloshing in a flexible tank using the unified FSM and the incompressible FSM with viscosity $\mu = 10^{-3}$ Pa-s and $\Delta t = 10^{-3}$ sec.	27
3.11	Tip deflection of left and right columns and middle deflection of the bottom beam using the unified FSM and the incompressible FSM with viscosity $\mu = 10^{-3}$ Pa-s and $\Delta t = 10^{-3}$ sec.	27
3.12	Convergence of velocity and pressure using unified FSM and incompressible FSM with viscosity $\mu = 10^{-3}$ Pa-s and time step $\Delta t = 10^{-3}$ sec.	28
3.13	Convergence of velocity and pressure using unified FSM and incompressible FSM with viscosity $\mu = 1.0$ Pa-s and time step $\Delta t = 10^{-3}$ sec.	29
3.14	Convergence of velocity and pressure using unified FSM and incompressible FSM with viscosity $\mu = 50$ Pa-s and time step $\Delta t = 10^{-3}$ sec.	29
3.15	Convergence of velocity and pressure using unified FSM and incompressible FSM with viscosity $\mu = 10^3$ Pa-s and time step $\Delta t = 10^{-3}$ sec.	30

3.16 Convergence of velocity and pressure using unified FSM and incompressible FSM with viscosity $\mu = 10^4$ Pa-s and time step $\Delta t = 10^{-3}$ sec.	30
3.17 Convergence of velocity and pressure using unified FSM and incompressible with viscosity $\mu = 10^3$ Pa-s and time step $\Delta t = 5 \times 10^{-5}$ sec.	31
3.18 Convergence of velocity and pressure using unified FSM and incompressible FSM with viscosity $\mu = 10^4$ Pa-s and time step $\Delta t = 5 \times 10^{-5}$ sec.	32
3.19 Convergence of velocity and pressure using unified FSM and incompressible FSM with viscosity $\mu = 10^4$ Pa-s and time step $\Delta t = 4 \times 10^{-6}$ sec.	32
4.1 Class diagram of multi-interpreter interface.	36
4.2 The implementation of <code>getDouble</code> in Python interpreter.	37
4.3 The implementation of <code>getDouble</code> in <i>Tcl</i> interpreter.	37
4.4 The implementation of the core API <code>OPS_Node</code>	38
4.5 Truss model for the Python interpreter.	39
4.6 Python scripts for nonlinear material truss analysis.	40
4.7 Python scripts for importing OpenSeesPy module.	41
4.8 Python scripts for plotting.	41
4.9 Python plotting for the nonlinear truss example.	42
4.10 Python code for adding fluid particles for the background mesh method.	42
4.11 Python code for a nonlinear material obstacle.	43
4.12 Python script for defining the background mesh.	43
4.13 Python code for running FSI analysis.	44
4.14 Python code for testing.	45
4.15 <i>Tcl</i> code for testing.	46
4.16 Part of benchmark results from Python.	51
4.17 Part of benchmark results from <i>Tcl</i>	52

1 Introduction

Recent hazards due to tsunami, storm surge, and hurricanes have caused significant damages to coastal infrastructure and bridges, such as 2005 Hurricane Katrina (Padgett et al. 2008) and 2011 Tohoku earthquake and tsunami (Suppasri et al. 2014). Indeed, the entire West Coast of the U.S. is vulnerable to distant tsunami and a potential strong earthquake associated with the Cascadia Subduction Zone, which would be followed by large tsunami impact. Many researchers have requested information on the fluid–structure interaction (FSI) simulation capabilities of OpenSees. In an effort to support the Pacific Earthquake Engineering Research Center’s (PEER) program in performance-based tsunami engineering (PBTE), the existing performance-based earthquake engineering (PBEE) methodology has been extended to FSI using the OpenSees platform to enhance its modeling ability, computing accuracy, and efficiency.

As the primary simulation tool for PEER, OpenSees’ focus has been primarily in in earthquake engineering and nonlinear structural analysis. Building upon existing functions in OpenSees, the first objective of this project was to further develop the FSI module to incorporate tsunami hazards into the analysis and assessment of buildings and bridges, as well as for sequential earthquake and tsunami hazards. The FSI simulation capabilities of OpenSees are based on the particle finite-element method (PFEM), which is a Lagrangian-based approach that conforms to pre-existing structural formulations available in OpenSees. By using the PFEM, the FSI analysis can be easily added in any existing OpenSees scripts without modifying the structural models. This is especially useful for researchers who have developed their structural models in OpenSees and want to test their models with tsunami loading.

In addition to the development of FSI modules, the second objective of this project was to expand the Python scripting capabilities of OpenSees, and make the framework more accessible to new generations of users. From their inception, the FSI modules in OpenSees have been based on Python scripting. To accomplish FSI simulations in OpenSees, Python commands have been added for a limited number of the pre-existing element and material commands, e.g., linear-elastic triangle elements and beam–column elements with *Concrete01/Steel01* fiber sections; that said, hundreds of constitutive models and element formulations remain to be incorporated under the Python umbrella. Although the original scripting language, *Tcl*, in OpenSees is string based, powerful, and easy to learn, it is not suitable for mathematical computations. Recent trends in scripting languages for engineer-

ing applications have embraced more general, scientific languages such as Python, which has evolved to a large community with numerous libraries for numerical computing, data analysis, scientific visualization, and web development. Extending OpenSees to Python will ensure that OpenSees keeps pace with new scripting developments as they are added by the scientific computing community.

The report will be organized in three main chapters. Chapter 1 introduces the background theories and algorithms, and the governing equations for the FSI analysis. The implementation of the FSI module in OpenSees and its relationship with exiting framework will be introduced in the Chapter 2. Chapter 3 focuses on the multi-interpreter interface in OpenSees, from which the Python interpreter is implemented.

2 Fluid-Structure Interaction

The FSI simulation in OpenSees was developed using the particle finite-element method (PFEM). Because the Lagrangian description has been widely used in structural analysis, the Lagrangian-based PFEM can be naturally coupled with existing structural formulations in OpenSees, leading to a monolithic system for the equations that govern FSI (Oñate et al. 2004; Cremonesi et al. 2010). The monolithic approach solves the combined fluid and structural domains simultaneously, and ensures equilibrium and compatibility across the FSI interface between the domains.

The advantage of using the PFEM is that it overcomes the complexity of coupling fluid and structure methods separately via staggered schemes (Oñate et al. 2011). The PFEM is also less sensitive to the exact location of the fluid–structure boundary, which can be a drawback to domain decomposition methods. These two factors, the easy coupling ability and arbitrary location of the FSI boundary, are especially important for the buildings and bridges that comprise coastal infrastructure. In earthquake engineering, which was initially the driving force in developing OpenSees, structures are usually represented as frame elements that can move arbitrarily in response to ground motion. There are also hundreds of other types of elements in OpenSees, and researchers are continually adding new elements. The strength of using the PFEM is that it allows FSI to be embedded in the OpenSees framework without modifying the elements.

Another advantage of using the PFEM is the accurate approximation of the wave loading and the interaction between fluid and structures. During a tsunami event, the interaction between tsunami waves and structures can be very complicated. The wave loading cannot be easily determined with initial wave speed and height, but largely depends on the structural dimensions and response. Particles are used to track the movements of the fluid, including large fluid bodies, breaking waves, and diverged currents around the structures. A structure may experience impact from different directions and sometime even from opposite directions of the tsunami waves.

Considering that the users of OpenSees are mainly composed of structural and geotechnical engineers, the FSI module in OpenSees was designed so that the user can minimize the effort required in running an FSI analysis by easily incorporating the module in their current structural models. The users should be able to add few lines in their existing scripts to include the fluid model and to set FSI analysis options without worrying the meshing, computation, and the interaction algorithms. This chapter introduces the underlying gov-

erning equations and finite-element discretization of the PFEM, the monolithic system of equations and fractional step solver of the FSI, and the mesh updating algorithms for the fluid and structure analysis.

2.1 Governing Equations

Conservation of linear momentum is enforced in both the fluid and structural domains, and can be written in the updated Lagrangian formulation as

$$\rho \dot{v}_i = \frac{\partial \sigma_{ij}}{\partial x_j} + \rho b_i \quad (2.1)$$

where ρ is the material density, v_i , x_i , and b_i are the velocity, coordinates, and body acceleration vectors, respectively, and σ_{ij} is the Cauchy stress tensor. Neumann boundary conditions prescribe normal stresses on the surface, Γ_t ,

$$\sigma_{ij} n_j = t_i \quad (2.2)$$

where t_i is the surface traction, and n_j is the unit vector normal to the boundary surface. The velocity and displacement are dependent variables of coordinates, and Dirichlet boundary conditions are imposed on displacements on the surface, Γ_v .

$$u_i = u_i^p \quad (2.3)$$

where u_i^p is the prescribed displacements. The intersection between Γ_t and Γ_v is the empty set, and their union is the entire boundary of the computational domain. As the simulation proceeds, the relationship between coordinates and displacements is

$$x_i = x_i^0 + u_i \quad (2.4)$$

where x_i^0 is the initial coordinates. The stress-strain relationship for the structural domain is assumed to be a general nonlinear function of displacement and velocity

$$\sigma_{ij} = \sigma_{ij}(u_i, v_i) \quad (2.5)$$

With this general form, it is straightforward to incorporate hysteresis and viscosity materials in OpenSees (Simo and Hughes 1998). For Newtonian fluids, the Cauchy stress is decomposed into spherical and deviatoric portions.

$$\sigma_{ij} = s_{ij} - p\delta_{ij} \quad (2.6)$$

where δ_{ij} is the Kronecker delta, and $p = \sigma_{ii}/3$ is the average stress (pressure), which is positive for compression. The deviatoric stress s_{ij} is defined in terms of the strain rate by

$$s_{ij} = 2\mu \left(\varepsilon_{ij} - \frac{1}{3}\varepsilon_v \delta_{ij} \right) \quad (2.7)$$

where μ is the viscosity, and ε_{ij} is the strain rate tensor,

$$\varepsilon_{ij} = \frac{1}{2} \left(\frac{\partial v_i}{\partial x_j} + \frac{\partial v_j}{\partial x_i} \right) \quad (2.8)$$

Conservation of mass in the structural domain can be written as

$$\rho J = \rho_0 \quad (2.9)$$

where ρ_0 is the density in the undeformed configuration, and J is the determinant of the deformation tensor as defined in Mase et al. (2009). Conservation of mass can be expressed as the divergence of the velocity field equal to the time rate of change in pressure,

$$\varepsilon_v = \varepsilon_{ii} = \frac{\partial v_i}{\partial x_i} = -\frac{1}{\kappa} \dot{p} \quad (2.10)$$

where κ is the bulk modulus. For incompressible flow, $\kappa = \infty$, Equation (2.10) becomes

$$\varepsilon_v = \varepsilon_{ii} = \frac{\partial v_i}{\partial x_i} = 0 \quad (2.11)$$

Nonlinear structural response is defined by the governing equations of linear momentum Equation (2.1), a general constitutive Equation (2.5), and mass conservation Equation (2.9). Likewise, the equations of linear momentum Equation (2.1), constitution Equation (2.7), and mass Equation (2.10) define the Newtonian fluid response.

2.2 Finite-Element Discretization

2.2.1 Structural equations

One of the challenges for the FSI computation in OpenSees is to make the FSI work with all elements in the framework. With this in mind, no specific structural elements should be assumed to discretize the structural governing equations in Equations (2.1), (2.5), and (2.9). By assuming a general structural element and applying the standard Galerkin formulation of the weighted residual method (Zienkiewicz et al. 2005), the discretized structural equations can be written as

$$\mathbf{M}_s \dot{\mathbf{v}}_s + \mathbf{K}_s \mathbf{v}_s + \mathbf{F}_s^{int} = \mathbf{F}_s \quad (2.12)$$

where \mathbf{v}_s is the structural velocities, and \mathbf{M}_s , \mathbf{K}_s , and \mathbf{F}_s^{int} and \mathbf{F}_s are the structural mass matrix, damping matrix, and internal and external force vectors, respectively. The internal force vector is a general nonlinear function of displacements and velocities that accounts for material and geometric nonlinearity for any type of element in OpenSees, such as beam–column configurations, shells, and plates.

2.2.2 Fluid equations

The same finite-element procedure can be applied to the equations governing fluids in Equations (2.1), (2.7), and (2.10). The MINI element (Arnold et al. 1984) is used for a mixed formulation of velocity and pressure to discretize the fluid domain. As a stable linear element, the MINI element overcomes the Inf-Sup condition for fully or nearly incompressible fluids (Gresho 1998) shown in Figure 2.1

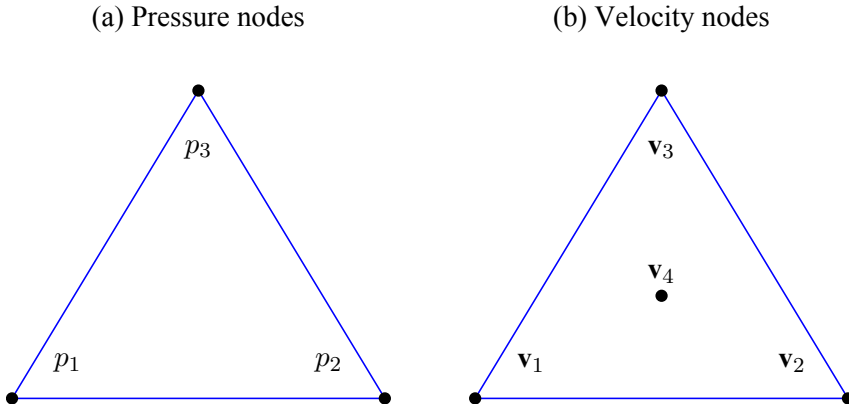


Figure 2.1: The MINI element.

The bubble node in Figure 2.1(b) enhances the velocity field with a cubic term and adds stability for the pressure interpolation. The discretized fluid equations can be written as

$$\mathbf{M}_f \dot{\mathbf{v}}_f + \mathbf{K}_f \mathbf{v}_f + \mathbf{F}_f^{int} = \mathbf{F}_f \quad (2.13)$$

$$\mathbf{M}_p \dot{\mathbf{p}} + \mathbf{G}_f^T \mathbf{v}_f = \mathbf{0} \quad (2.14)$$

where \mathbf{v}_f and \mathbf{p} are the fluid velocities and pressures, and \mathbf{M}_f , \mathbf{K}_f , and \mathbf{F}_f^{int} and \mathbf{F}_f are the fluid mass matrix, viscous matrix, and internal and external force vectors, respectively. The fluid internal force vector corresponds to the pressure gradients.

$$\mathbf{F}_f^{int} = -\mathbf{G}_f \mathbf{p} \quad (2.15)$$

where \mathbf{G}_f is the gradient operator, and the pressure mass matrix \mathbf{M}_p is valid only for quasi-incompressible flow, whose bulk modulus, κ , is finite.

2.2.3 Monolithic system

As a monolithic system that governs FSI, the compatibility along the interface of FSI is satisfied through the nodes connected to both the fluid and structural domains. These nodes are identified as interface nodes, whose contributions appear in both fluid and structural

equations. For the structural equation, the interface equations are extracted from Equation (2.12) and assigned additional i and s subscripts

$$\mathbf{M}_{ss}\dot{\mathbf{v}}_s + \mathbf{M}_{si}\dot{\mathbf{v}}_i + \mathbf{K}_{ss}\mathbf{v}_s + \mathbf{K}_{si}\mathbf{v}_i + \mathbf{F}_s^{int} = \mathbf{F}_s \quad (2.16)$$

$$\mathbf{M}_{is}\dot{\mathbf{v}}_s + \mathbf{M}_{ii}^s\dot{\mathbf{v}}_i + \mathbf{K}_{is}\mathbf{v}_s + \mathbf{K}_{ii}^s\mathbf{v}_i + \mathbf{F}_i^{int} = \mathbf{F}_i^s \quad (2.17)$$

where $\dot{\mathbf{v}}_i$ and \mathbf{v}_i are the acceleration and velocity vectors of the interface nodes, respectively. Similarly, the interface equations are extracted from Equations (2.13) and (2.14) for the fluid domain and given additional i and j subscripts

$$\mathbf{M}_{ff}\dot{\mathbf{v}}_f + \mathbf{K}_{ff}\mathbf{v}_f - \mathbf{G}_f\mathbf{p} = \mathbf{F}_f \quad (2.18)$$

$$\mathbf{M}_{ii}^f\dot{\mathbf{v}}_i + \mathbf{K}_{ii}^f\mathbf{v}_i - \mathbf{G}_i\mathbf{p} = \mathbf{F}_i^f \quad (2.19)$$

$$\mathbf{M}_p\dot{\mathbf{p}} + \mathbf{G}_f^T\mathbf{v}_f + \mathbf{G}_i^T\mathbf{v}_i = \mathbf{0} \quad (2.20)$$

where the off-diagonal terms in the mass and viscous matrices, \mathbf{M}_{fi} , \mathbf{M}_{if} , \mathbf{K}_{fi} , \mathbf{K}_{if} , have disappeared due to diagonalization of the mass matrix and formulation of the MINI element. The interface equations in Equations (2.17) and (2.19) are combined to satisfy equilibrium on the FSI interface. The combined monolithic system for the FSI can be written as

$$\mathbf{M}_{ss}\dot{\mathbf{v}}_s + \mathbf{M}_{si}\dot{\mathbf{v}}_i + \mathbf{K}_{ss}\mathbf{v}_s + \mathbf{K}_{si}\mathbf{v}_i + \mathbf{F}_s^{int} = \mathbf{F}_s \quad (2.21)$$

$$\mathbf{M}_{is}\dot{\mathbf{v}}_s + \mathbf{K}_{is}\mathbf{v}_s + \mathbf{M}_{ii}\dot{\mathbf{v}}_i + \mathbf{K}_{ii}\mathbf{v}_i + \mathbf{F}_i^{int} - \mathbf{G}_i\mathbf{p} = \mathbf{F}_i \quad (2.22)$$

$$\mathbf{M}_{ff}\dot{\mathbf{v}}_f + \mathbf{K}_{ff}\mathbf{v}_f - \mathbf{G}_f\mathbf{p} = \mathbf{F}_f \quad (2.23)$$

$$\mathbf{M}_p\dot{\mathbf{p}} + \mathbf{G}_f^T\mathbf{v}_f + \mathbf{G}_i^T\mathbf{v}_i = \mathbf{0} \quad (2.24)$$

where \mathbf{M}_{ii} , \mathbf{K}_{ii} , and \mathbf{F}_i are the combined matrices and vector at the interface

$$\mathbf{M}_{ii} = \mathbf{M}_{ii}^s + \mathbf{M}_{ii}^f \quad (2.25)$$

$$\mathbf{K}_{ii} = \mathbf{K}_{ii}^s + \mathbf{K}_{ii}^f \quad (2.26)$$

$$\mathbf{F}_i = \mathbf{F}_i^s + \mathbf{F}_i^f \quad (2.27)$$

The combined system in Equations (2.21), (2.22), (2.23), and (2.24) should be further discretized in the time domain and solved using a nonlinear algorithm, which will be introduced in the following sections.

2.3 Time-Domain Discretization

A Backward Euler time integration is employed for the time-domain discretization. The displacement and acceleration are expressed in terms of the velocity at the current time step, and the displacement and velocity at the previous time step,

$$\mathbf{u}_{n+1} = \mathbf{u}_n + \Delta t \mathbf{v}_{n+1} \quad (2.28)$$

$$\dot{\mathbf{v}}_{n+1} = \frac{\mathbf{v}_{n+1} - \mathbf{v}_n}{\Delta t} \quad (2.29)$$

The linearization of Equations (2.28) and (2.29) gives the updated formula when the velocity increment is computed:

$$\mathbf{u}_{n+1}^{j+1} = \mathbf{u}_{n+1}^j + \Delta t \Delta \mathbf{v}_{n+1} \quad (2.30)$$

$$\mathbf{v}_{n+1}^{j+1} = \mathbf{v}_{n+1}^j + \Delta \mathbf{v}_{n+1} \quad (2.31)$$

$$\dot{\mathbf{v}}_{n+1}^{j+1} = \dot{\mathbf{v}}_{n+1}^j + \frac{1}{\Delta t} \Delta \mathbf{v}_{n+1} \quad (2.32)$$

where n is the time step number, and j is the iteration number. The time integration of pressures can be written in a similar form:

$$\dot{\mathbf{p}}_{n+1} = \frac{\mathbf{p}_{n+1} - \mathbf{p}_n}{\Delta t} \quad (2.33)$$

$$\mathbf{p}_{n+1}^{j+1} = \mathbf{p}_{n+1}^j + \Delta \mathbf{p}_{n+1} \quad (2.34)$$

$$\dot{\mathbf{p}}_{n+1}^{j+1} = \dot{\mathbf{p}}_{n+1}^j + \frac{1}{\Delta t} \Delta \mathbf{p}_{n+1} \quad (2.35)$$

Although using a different time integration is possible, the Backward Euler time integration is stable and keeps the original structure in the combined system.

2.4 Nonlinear Solution Algorithm

The combined system in Equations (2.21), (2.22), (2.23), and (2.24) is composed of nonlinear equations because of the general nonlinear material for structures and geometric nonlinearity for the fluid and structure. Solution of the nonlinear equations is obtained using the Newton–Raphson algorithm, which writes equations in the residual form:

$$\mathbf{r}_s = \mathbf{F}_s - (\mathbf{M}_{ss} \dot{\mathbf{v}}_s + \mathbf{K}_{ss} \mathbf{v}_s + \mathbf{M}_{si} \dot{\mathbf{v}}_i + \mathbf{K}_{si} \mathbf{v}_i + \mathbf{F}_s^{int}) \quad (2.36)$$

$$\mathbf{r}_i = \mathbf{F}_i - (\mathbf{M}_{is} \dot{\mathbf{v}}_s + \mathbf{K}_{is} \mathbf{v}_s + \mathbf{M}_{ii} \dot{\mathbf{v}}_i + \mathbf{K}_{ii} \mathbf{v}_i + \mathbf{F}_i^{int} - \mathbf{G}_i \mathbf{p}) \quad (2.37)$$

$$\mathbf{r}_f = \mathbf{F}_f - (\mathbf{M}_{ff} \dot{\mathbf{v}}_f + \mathbf{K}_{ff} \mathbf{v}_f - \mathbf{G}_f \mathbf{p}) \quad (2.38)$$

$$\mathbf{r}_p = -(\mathbf{M}_p \dot{\mathbf{p}} + \mathbf{G}_f^T \mathbf{v}_f + \mathbf{G}_i^T \mathbf{v}_i) \quad (2.39)$$

Following the procedure of the Newton–Raphson algorithm, the derivative of the residual is obtained with respect to the velocity and pressure unknowns, at which point the velocity and pressure increments can be computed as follows:

$$\mathbf{K}_T \begin{bmatrix} \Delta \mathbf{v}_s \\ \Delta \mathbf{v}_i \\ \Delta \mathbf{v}_f \\ \Delta \mathbf{p} \end{bmatrix} = \begin{bmatrix} \mathbf{r}_s \\ \mathbf{r}_i \\ \mathbf{r}_f \\ \mathbf{r}_p \end{bmatrix} \quad (2.40)$$

where \mathbf{K}_T is the combined tangent stiffness matrix for the structural interface and fluid velocities and pressures.

$$\mathbf{K}_T = - \left(\frac{\partial [\mathbf{r}_s \ \mathbf{r}_i \ \mathbf{r}_f \ \mathbf{r}_p]}{\partial [\mathbf{v}_s \ \mathbf{v}_i \ \mathbf{v}_f \ \mathbf{p}]} \right)^{-1} = \begin{bmatrix} \mathbf{K}_{Tss} & \mathbf{K}_{Tsi} & \mathbf{0} & \mathbf{0} \\ \mathbf{K}_{Tis} & \mathbf{K}_{Tii} & \mathbf{0} & -\mathbf{G}_i \\ \mathbf{0} & \mathbf{0} & \mathbf{K}_{Tff} & -\mathbf{G}_f \\ \mathbf{0} & \mathbf{G}_i^T & \mathbf{G}_f^T & \mathbf{K}_{Tpp} \end{bmatrix} \quad (2.41)$$

The matrices \mathbf{K}_{Tss} and \mathbf{K}_{Tsi} are tangents of the structural residual to the structural and interface velocities:

$$\mathbf{K}_{Tss} = -\frac{\partial \mathbf{r}_s}{\partial \mathbf{v}_s} = \frac{1}{\Delta t} \mathbf{M}_{ss} + \mathbf{K}_{ss} + \Delta t \frac{\partial \mathbf{F}_s^{int}}{\partial \mathbf{v}_s} \quad (2.42)$$

$$\mathbf{K}_{Tsi} = -\frac{\partial \mathbf{r}_s}{\partial \mathbf{v}_i} = \frac{1}{\Delta t} \mathbf{M}_{si} + \mathbf{K}_{si} + \Delta t \frac{\partial \mathbf{F}_s^{int}}{\partial \mathbf{v}_i} \quad (2.43)$$

Likewise, the matrices \mathbf{K}_{Tis} and \mathbf{K}_{Tii} are tangents of the interface residual to the structural and interface velocities:

$$\mathbf{K}_{Tis} = -\frac{\partial \mathbf{r}_i}{\partial \mathbf{v}_s} = \frac{1}{\Delta t} \mathbf{M}_{is} + \mathbf{K}_{is} + \Delta t \frac{\partial \mathbf{F}_i^{int}}{\partial \mathbf{v}_s} \quad (2.44)$$

$$\mathbf{K}_{Tii} = -\frac{\partial \mathbf{r}_i}{\partial \mathbf{v}_i} = \frac{1}{\Delta t} \mathbf{M}_{ii} + \mathbf{K}_{ii} + \Delta t \frac{\partial \mathbf{F}_i^{int}}{\partial \mathbf{v}_i} \quad (2.45)$$

The matrix \mathbf{K}_{Tff} , which is the tangent of the fluid residual to the fluid velocity, is not connected to structural and interface tangents:

$$\mathbf{K}_{Tff} = -\frac{\partial \mathbf{r}_f}{\partial \mathbf{v}_f} = \frac{1}{\Delta t} \mathbf{M}_{ff} + \mathbf{K}_{ff} \quad (2.46)$$

The combined system, shown in Equation (2.41), connects the structural and fluid domains through the interface pressure gradients matrix \mathbf{G}_i , which represents the wave loading applied on the structures. The matrix \mathbf{K}_{Tpp} is the tangent of the pressure residual to the fluid pressures, which accounts for compressibility and stability of the fluid formulation.

$$\mathbf{K}_{Tpp} = -\frac{\partial \mathbf{r}_p}{\partial \mathbf{v}_p} = \frac{1}{\Delta t} \mathbf{M}_p \quad (2.47)$$

In each iteration of the nonlinear solution procedure, the velocity and pressure increments are computed by Equation (2.40), and the displacements, velocities, accelerations, and pressures are updated, as shown in Equation (2.30)–Equation (2.35). The convergence is tested by checking the increment and residual vectors in Equation (2.40). If they are smaller than preset tolerances, the combined system in Equations (2.36), (2.37), (2.38), and (2.39) is considered to be satisfied, and the solutions are obtained for the current time step.

2.5 Various Solvers for FSI in OpenSees

The monolithic matrix in Equation (2.41) is ill-conditioned due to the coupling of the velocity and pressure fields, making it difficult to obtain a stable numerical solution for the incremental velocities and pressures. There are two solvers available in OpenSees to solve Equation (2.40) efficiently, with a stable solution depending on assumptions of the fluid. Each of them will be introduced in the following sections.

2.5.1 Incompressible fractional step solver

The fractional step method (FSM) is widely used in the PFEM (Oñate et al. 2004; Aubry et al. 2006; Idelsohn and Oñate 2010; Idelsohn et al. 2009) to solve Equation (2.40). Because the FSM segregates the velocities and pressures into smaller systems of equations, it is well-conditioned to overcome the difficulties in solving the combined system. By assuming incompressible and near-inviscid fluid in Equation (2.46), the viscous matrix \mathbf{K}_{ff} can be ignored, and the mass matrix \mathbf{M}_{ff} can be lumped. At which point, the tangent matrix \mathbf{K}_{Tff} becomes diagonal and trivial to invert; the solution of fluid velocity increments are now available from Equation (2.40)

$$\Delta \mathbf{v}_f = \Delta \mathbf{v}_f^* + \mathbf{K}_{Tff}^{-1} \mathbf{G}_f \Delta \mathbf{p} \quad (2.48)$$

where $\Delta \mathbf{v}_f^* = \mathbf{K}_{Tff}^{-1} \mathbf{r}_f$ is the predictor velocity increments for the fluid. By substituting Equation (2.48) into Equation (2.40), the combined system can be solved in three steps:

1. Compute predictor velocity increments for the structure ($\Delta \mathbf{v}_s^*$), interface ($\Delta \mathbf{v}_i^*$), and fluid ($\Delta \mathbf{v}_f^*$). The predictor of fluid velocity increment ($\Delta \mathbf{v}_f^*$) is trivial to solve, as

- seen in Equation (2.48). An efficient computation for structural and interface pre-dictor velocity increments has been shown in Zhu and Scott (2014);
2. Solve for pressure increments ($\Delta\mathbf{p}$) from the predicted velocity increments; and
 3. Correct the velocity increments for the structural ($\Delta\mathbf{v}_s$), interface ($\Delta\mathbf{v}_i$), and fluid ($\Delta\mathbf{v}_f$) using the pressure increments ($\Delta\mathbf{p}$) using Equation (2.48) found in Step 2.

Further information on the mathematical formulations for the three steps of the FSM can be found in Zhu and Scott (2014). The advantage of using the incompressible FSM solver is as follows: (1) it can incorporate the flexibility of the structure by including the added-mass effects; and (2) it maintains the incompressibility without mass loss. These two factors are important for tsunami simulations using OpenSees, which usually contain flexible bridge and building structures. The assumption of incompressible fluid is also adequate for real analyses of tsunami waves.

2.5.2 Unified fractional step solver

For incompressible and near-inviscid fluid, the inversion of the matrix \mathbf{K}_{Tff} is trivial, and the matrix \mathbf{M}_p vanishes, making the second step in the FSM easier to perform. For general fluid, such as oil and air, the inversion is too expensive, and the compressibility of fluid must be considered. To this end, a unified fractional step solver is proposed to provide an alternative means of solving Equation (2.40).

The unified solver assumes a quasi-incompressible fluid formulation, which maintains the non-zero matrix \mathbf{M}_p and a general matrix \mathbf{K}_{Tff} . Instead of computing predictor velocities in the regular FSM, the unified solver calculates predictor pressure by the inversion of the matrix \mathbf{K}_{Tpp} . Since the matrix \mathbf{K}_{Tpp} is provided by the pressure mass matrix \mathbf{M}_p —which can be lumped whether the structure is linear or nonlinear, or the fluid is viscous or inviscid—the solution of pressure increments can be obtained from Equation (2.40)

$$\Delta\mathbf{p} = \Delta\mathbf{p}^* - \mathbf{K}_{Tpp}^{-1} \mathbf{G}_i^T \Delta\mathbf{v}_i - \mathbf{K}_{Tpp}^{-1} \mathbf{G}_f^T \Delta\mathbf{v}_f \quad (2.49)$$

where $\Delta\mathbf{p}^* = \mathbf{K}_{Tpp}^{-1} \mathbf{r}_p$ is the predictor pressure increment. By substituting Equation (2.49) into Equation (2.40), the combined system can be solved by reversing the three steps:

1. Compute predictor pressure increments ($\Delta\mathbf{p}^*$) with Equation (2.49);
2. Solve for velocity increments ($\Delta\mathbf{v}_s$, $\Delta\mathbf{v}_i$, $\Delta\mathbf{v}_f$) from the predicted pressure increments Zhu and Scott (2017); and
3. Correct the pressure increments ($\Delta\mathbf{p}$) using the velocity increments ($\Delta\mathbf{v}_s$, $\Delta\mathbf{v}_i$, $\Delta\mathbf{v}_f$) found in Step 2 by Equation (2.49).

Further information about the unified solution can be found in Zhu and Scott (2017). Although the unified FSM can solve more general FSI problems than the incompressible FSM and considers the compressibility of fluid, it has a larger system of equations and requires more computational effort. An additional advantage of the unified solver is its application for performing a sensitivity analysis, which will be introduced in the next section.

2.6 Domain Meshing for FSI

One of the challenges in using a Lagrangian-based FSI is the mesh updating for the fluid domain. In a Lagrangian description, the nodes and particles are moving with the flow. The fluid elements will become distorted and slow down the convergence. To maintain decent mesh quality, the PFEM remeshes the entire domain using efficient algorithms, such as the Delaunay Triangulation (Calvo et al. 2003). Although meshing is traditionally considered computationally expensive, the PFEM has simplified the meshing and sped up its operation. The meshing does not start from the geometry of the domain as is done with traditional mesh algorithms; it is dependent on the positions of moving particles only. There are two meshing methods available for use with the PFEM: the moving and the background mesh method, both of which are introduced next.

2.6.1 Moving mesh method

A moving mesh method considers the finite-element nodes equivalent as particles, which are used to transport fluid properties along the flow. These finite-element nodes are both mesh nodes and transporting particles. When moving through the domain, the locations of the finite-element nodes are arbitrary. A Delaunay Triangulation (DT) is needed to construct the mesh, based only on the nodal positions in the previous time step. Since the computing effort of a DT has been proven to be minimal (Watson 1981), it is possible to remesh in every time step. The procedure of the moving mesh method is demonstrated in the figures below.

As shown in Figure 2.2, interface particles are part of the structure, which interact with fluid particles. Given the particles, the DT can be constructed to connect all particles in the domain.

As seen in Figure 2.3, the entire domain is triangulated. Even those regions that are not part of the structural or fluid domain are included; thus, small and distorted triangles can be found in some areas. An extra step has been taken herein to identify the boundary of the domain and remove unnecessary triangles. This algorithm is called the Alpha Shape Method (Edelsbrunner and Mücke 1994), which decides if a triangle is valid or not based on its size and shape. The final mesh is shown in Figure 2.4

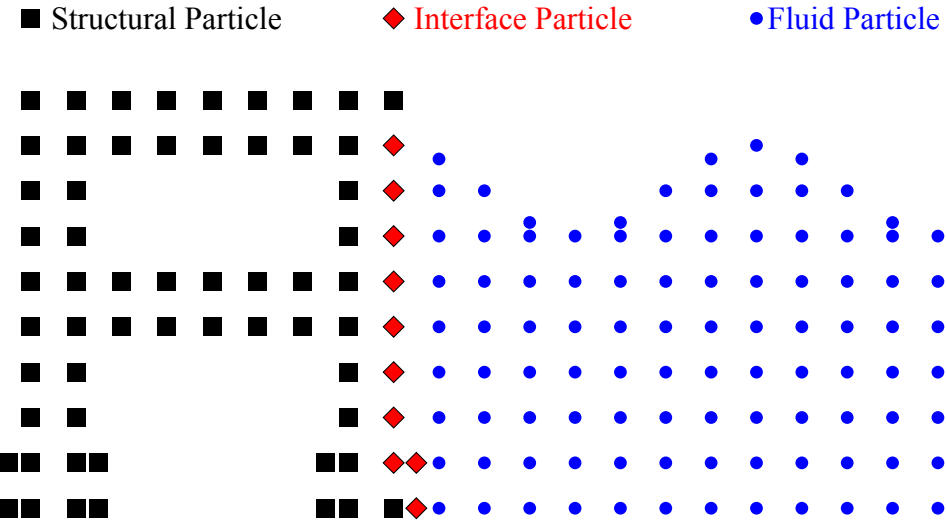


Figure 2.2: A cloud of FSI particles.

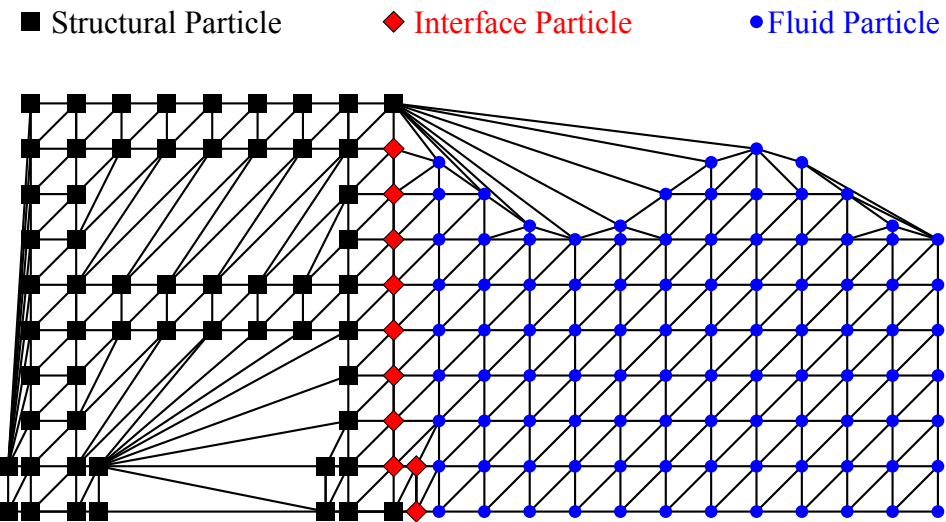


Figure 2.3: Delaunay Triangulation of the cloud of FSI particles.

■ Structural Particle ♦ Interface Particle • Fluid Particle

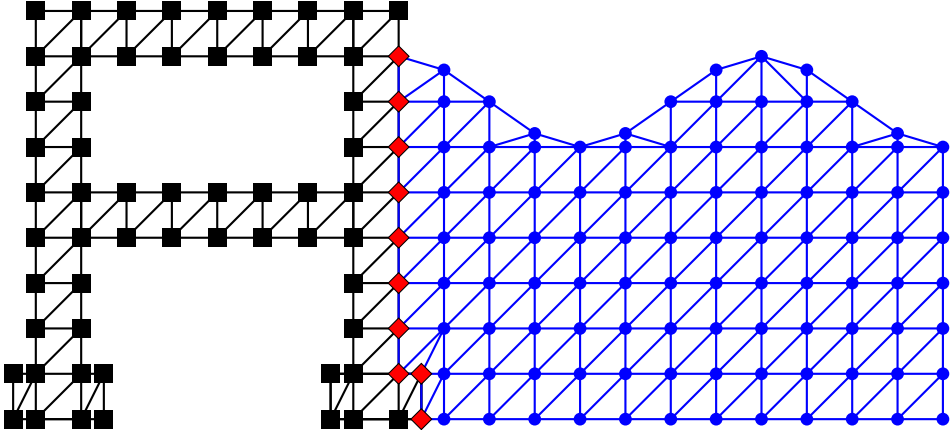


Figure 2.4: Moving mesh of the cloud of FSI particles.

The advantage of the moving mesh is twofold: it is efficient in terms of mesh updating, and it is flexible for any geometry of the structure and boundary conditions; however, as shown in Figure 2.4, small elements are formed since it is inevitable that fluid particles move close to each other. In a Lagrangian formulation, the smallest element controls the size of the time steps. As a result, a strict limit should be placed on the time step sizes in order to obtain a converged solution. This limitation can be overcome by the following background mesh method.

2.6.2 Background mesh method

The background mesh method separates the functions of the finite-element nodes and moving particles so that finite-element nodes do not have to move with the flow and can be fixed in the background. The fixed mesh circumvents the problem of small and distorted elements in the moving mesh, but needs more particles to transport the fluid properties.

A background mesh method with a fixed finite-element mesh has been used by Becker et al. (2015) for rapid generation of mesh in fluid–structure interaction (FSI) analysis. Since triangular structural and fluid elements are used together in the fixed mesh, the structural and fluid domains are uniformly meshed; therefore, no local remeshing is needed around structures. If a general structure, such as coastal infrastructure, cannot always be modeled with a fixed mesh, then the local mesh around the structure should be reconstructed to connect the structure to the fixed mesh. The modified background mesh mixes the fixed and moving mesh, benefiting from the use of both methods.

As shown in Figure 2.5, a cloud of fluid particles are placed on the background. Based on the locations of the fluid particles, a fixed background mesh is created with fluid ele-

● Fluid Particle

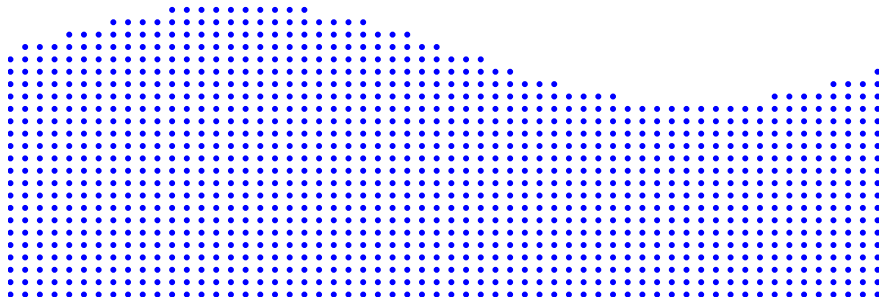


Figure 2.5: A cloud of fluid particles.

● Fluid Particle

■ Fluid Nodes

△ Fluid Elements

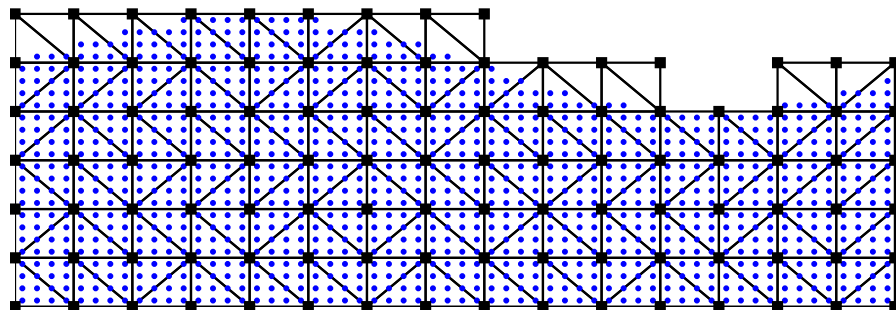


Figure 2.6: The fixed fluid mesh based on the fluid particles.

ments and nodes.

As shown in Figure 2.6, the fluid particles and nodes are separated in the fixed mesh. The fluid nodes are always fixed on the grids in the background, and the fluid elements are of good quality.

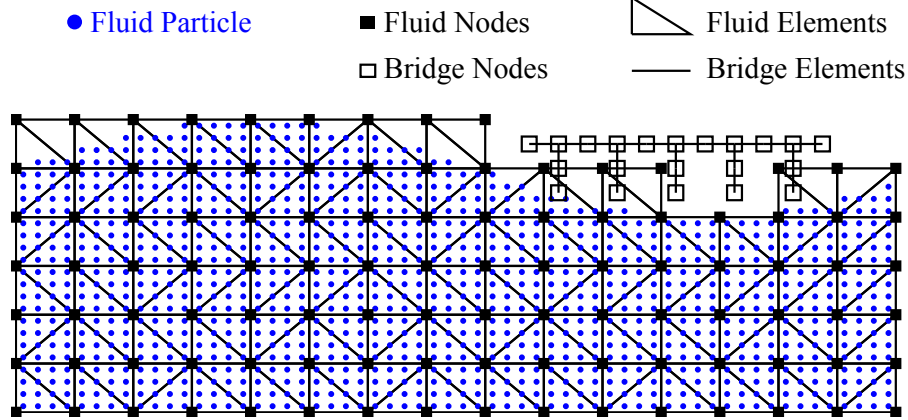


Figure 2.7: The fixed-fluid mesh with structure.

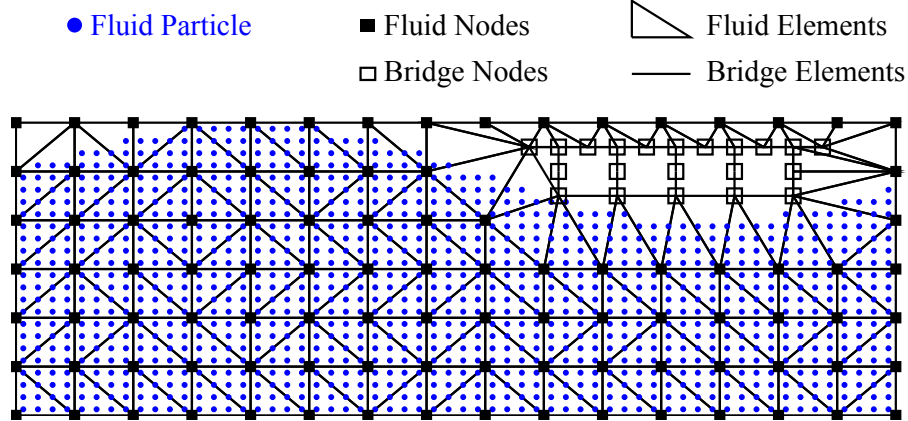


Figure 2.8: The Delaunay Triangulation between fixed-fluid mesh and structure.

As shown in Figure 2.7, a bridge structure is placed on the fixed mesh. Since part of the structural mesh overlaps with the fixed mesh, the local fixed mesh around the structure has to be removed and remeshed. Then a DT can be performed in the local area; note that some triangles are obviously not part of the mesh; see Figure 2.8. Instead of using the Alpha Shape Method, an easy and straightforward way to identify unnecessary triangles is to find and remove the empty triangles that have no particle. The final background mesh is shown in Figure 2.9.

All the background information, governing equations, solution algorithms, numerical solvers, and mesh updating methods have been introduced in this chapter. In the next

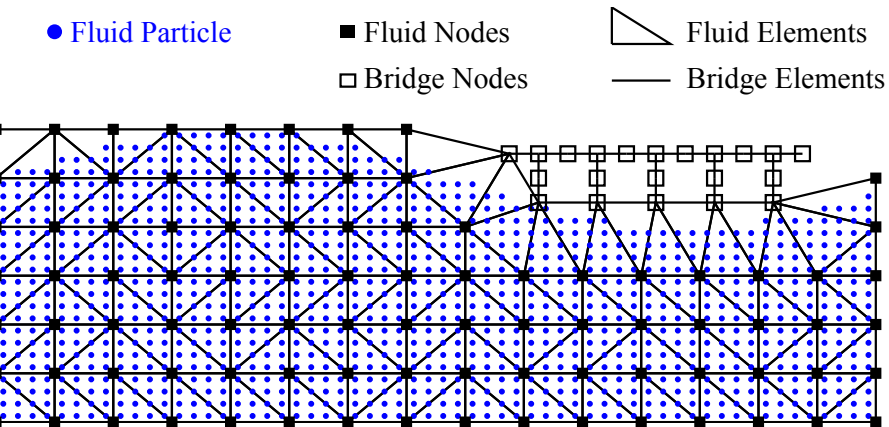


Figure 2.9: The background mesh with fixed fluid mesh and structure.

chapter, examples implementing the FSI in OpenSees will be introduced.

3 Implementation of FSI in OpenSees

The software design of OpenSees favors object composition as the mechanism that enables flexibility and extensibility of the framework. At the highest level of the OpenSees framework, the `class Domain` contains components (nodes, elements, loads, constraints, etc.) that are created and added to the domain through an input script. The state of each domain component is computed by the `class Analysis`, which is composed of an equation solver, solution algorithm, time integrator, constraint handler, and element and nodal assembly objects. Complete details of the design of OpenSees for nonlinear finite-element analysis are given in McKenna et al. (2010). Only the details of how the FSI implementation has been successfully achieved in OpenSees are introduced herein.

Since it was primarily designed to solve structural dynamics problems, there are two major challenges to the implementation of the FSI in OpenSees. The first challenge arises from the mesh updating at every time step. Since meshing is usually done at the script level in OpenSees, a built-in meshing function needs to be implemented for the mesh updating in the FSI. The second challenge involves solving the linear system of equations via the FSM solvers, which requires multiple equation solutions using the submatrices. Although OpenSees contains a flexible set of equation solvers, there is an implicit assumption that only one equation solution takes place during each iteration within a time step.

3.1 Domain Meshing

As shown in Figure 3.1, the `class Domain` stores model components, such as `Node`, `Element`, and `PressureConstraint`. To create finite-element nodes and elements, the `class Mesh` is introduced to the OpenSees framework, which is further inherited by the `class TriMesh` to generate fluid nodes and elements.

In the fluid analysis, each instance of the `class PFEMElement2DBubble` and the `class PFEMElement2DCompressible` are responsible for computing and returning its mass, stiffness, and damping matrices and resisting force vector for the incompressible and the quasi-incompressible flows.

The implementation of the `class Mesh` is shown in Figure 3.2. Four sub-classes were created for four different shapes of the elements. The `class LineMesh` is for line elements, such as beams and columns. Triangular and quadrilateral elements are meshed by

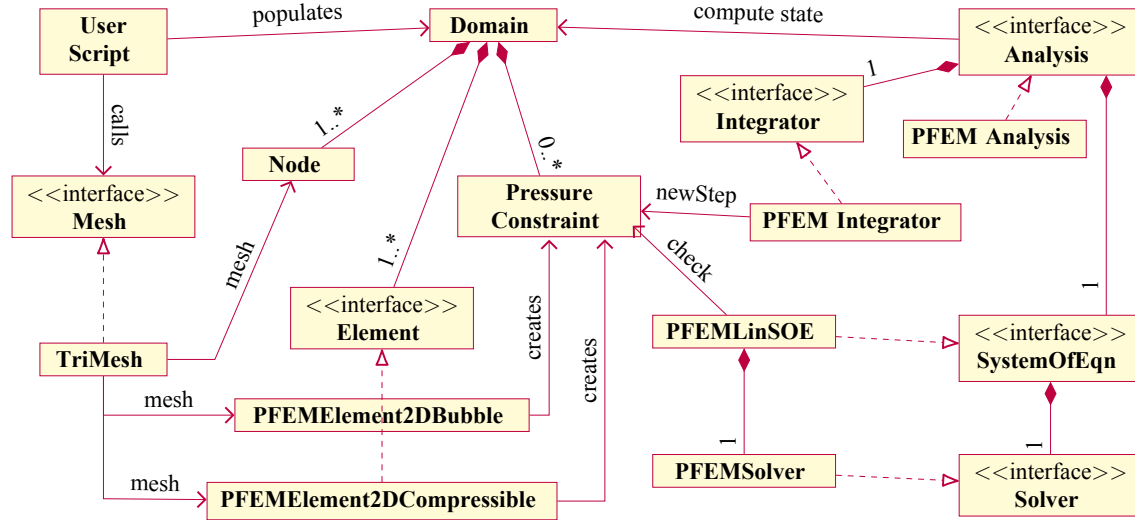


Figure 3.1: Class diagram of the FSI implementation in OpenSees framework.

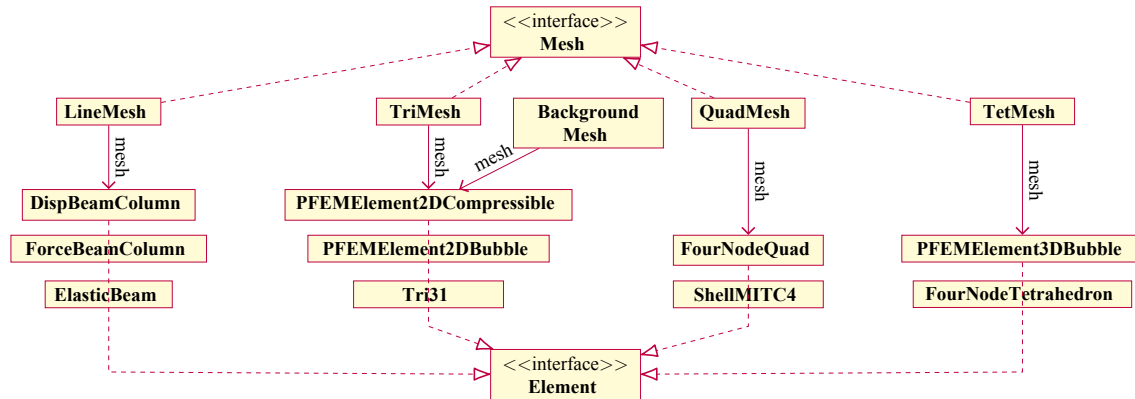


Figure 3.2: `class Mesh` in OpenSees framework.

the `class TriMesh` and `class QuadMesh`, including both fluid and solid elements. The `class TetMesh` is a three-dimensional (3D) tetrahedral elements mesher. For other element shapes, the corresponding mesher can be easily added as a subclass of Mesh. The `class TriMesh` implements the moving mesh method introduced in Section 2.6.1. The background mesh method was implemented in a standalone `class BackgroundMesh`, which performed the same task to create a triangular mesh as the TriMesh.

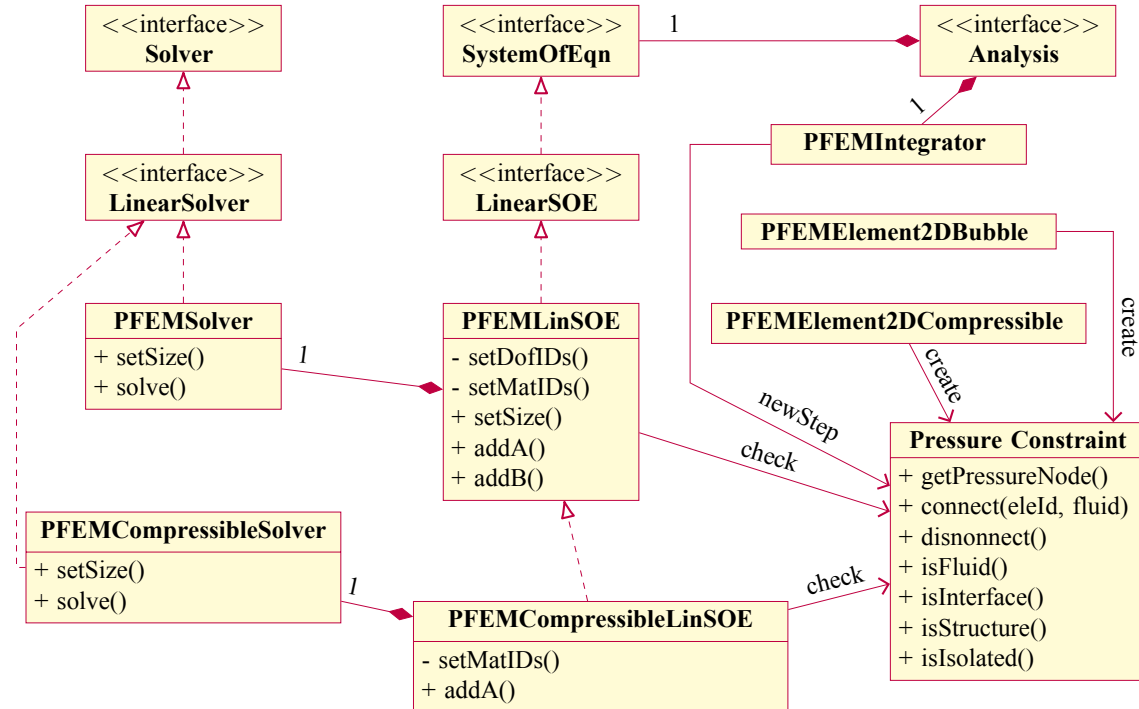


Figure 3.3: FSM solvers in OpenSees framework.

When fluid elements are added to the domain, the `PressureConstraint` objects are created to identify each node as belonging to the fluid and structural domains, the interface between these domains, or as separate from any domain. Two groups of element tags (one for fluid and one for structure) are stored in a `PressureConstraint` object and set via the `connect/disconnect` pair of methods; see Figure 3.3. Methods such as `isStructure` return the node type based on its connections and allows elements to determine their state accordingly. Another important task of the `PressureConstraint` object is to store a pointer able to identify a `Node` object internally to keep track of the unknown factors of the pressure. This is in addition to external node objects that keep track of the displacement, velocity, and acceleration of all fluid and structural nodes. The pointer to the pressure node can be returned through the `getPressureNode` method, so that fluid elements can obtain the nodal state and then return their contributions to the governing equations.

3.2 FSM Solvers

With a fluid mesh in place, the `class PFEMIntegrator` is able to implement the implicit Euler time integration method using particle velocity as the primary unknown along with the pressure; see Figure 3.1. At each time step, the integrator calls `PressureConstraint` objects to update the state of each isolated particle and to assemble the governing equations for particles that are connected to a mesh of fluid elements. The `class PFEMAnalysis` sets the maximum and minimum time steps for the simulation, and may reduce the time step if convergence is not achieved.

The `class PressureConstraint` serves as a bridge between the analysis and model classes of OpenSees in order to link the finite-element model to the predictor–corrector approach of the FSM. In terms of the analysis, new implementations of the `LinearSOE` and `LinearSolver` interfaces shown Figure 3.3 are required in order to carry out the FSM and partition the matrices in Equation (2.41), which are based on the model information from `PressureConstraint` objects. To this end, the `setDofIDs` method of the `class PFEMLinSOE`, which inherits the `LinearSOE` interface, obtains the node types from the `PressureConstraint` objects, and sets the matrix partitions and assigns equation numbers. The `setMatIDs` method is then called in order to initialize the partitioned matrices and residual vector of Equation (2.40) for assembly via implementation of the `addA` and `addB` methods. Using the partitioned matrices stored in the `PFEMLinSOE` object, the `class PFEMSolver`, which implements the `LinearSolver` interface, carries out the incompressible FSM and returns the solution for incremental velocities and pressures. The unified FSM solver is implemented in the `class PFEMCompressibleLinSOE` and the `class PFEMCompressibleSolver`.

3.3 Examples

The following section presents examples to verify, validate, and demonstrate FSI’s implementation in OpenSees.

3.3.1 Moving mesh model of a dam break as an elastic obstacle

This example verifies that the FSI implementation that has incorporated a moving and background mesh, and compares it to results obtained using different FSI numerical methods. The moving mesh model is of a dam break on an elastic obstacle fixed to be bottom of a tank; see Figure 3.4. The characteristic length, L , is equal to 0.146 m, and the elastic obstacle is $b = 0.012$ m side and $20b/3 = 0.08$ m high. The elastic obstacle is modeled as a co-rotational mesh of beam elements having a density of $\rho_s = 2500$ kg/m³, an elastic modulus of $E = 10^6$ Pa, and a Poisson ratio of $\gamma = 0$. The fluid density is $\rho_f = 1000$ kg/m³, and its viscosity is $\mu = 0.001$ kg/ms.

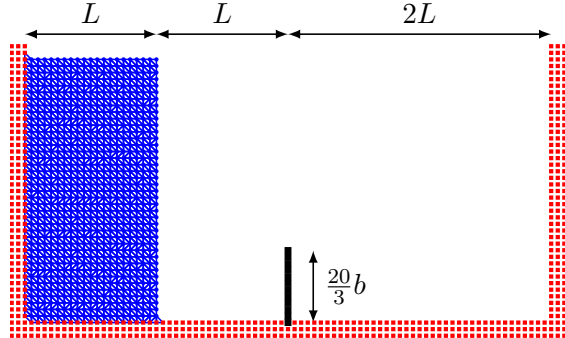


Figure 3.4: Elastic obstacle with moving mesh.

Although experimental data are not available, this example has been studied by several researchers (Ryzhakov et al. 2010; Idelsohn et al. 2008; Rafiee and Thiagarajan 2009; Walhorn et al. 2005), and provides a good point of comparison for the FSI implementation with previous simulation results. Snapshots of the dam-break simulation using the incompressible FSM with moving mesh are shown in Figure 3.5. To highlight the final displaced shape of the elastic obstacle, the fluid mesh was not included in the final snapshot of Figure 3.5.

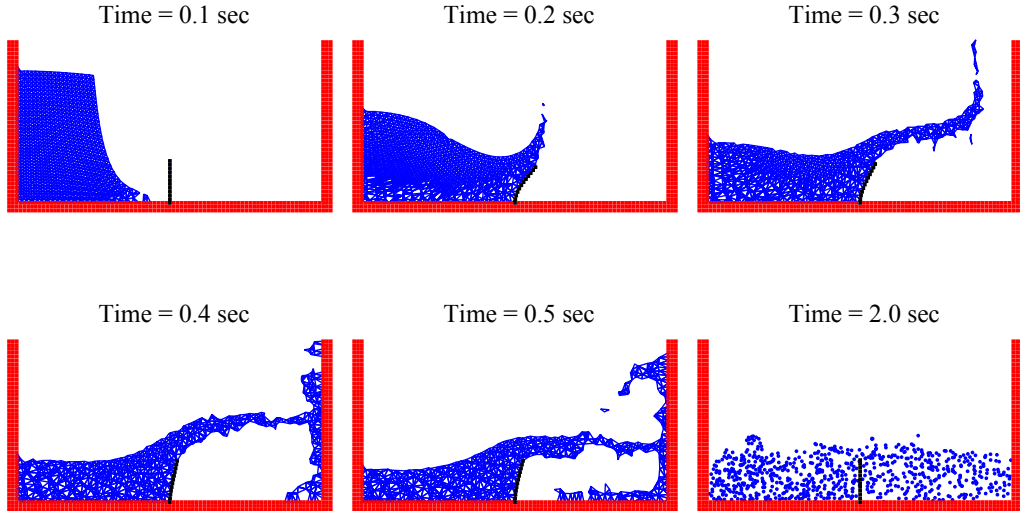


Figure 3.5: Snapshots of a dam break as an elastic obstacle with moving mesh.

The same example is also run with the background mesh method using the incompressible FSM. The snapshots of the background mesh simulation at the same time instances are shown in Figure 3.6. To elucidate the point, the background mesh has been hidden, and only fluid particles and structural mesh are presented. The walls are also not shown in Figure 3.6 since the wall nodes are part of the hidden background mesh. By comparing the Figure 3.5 and Figure 3.6, the displaced shape of the elastic obstacle and the progress of the water movement matches qualitatively.

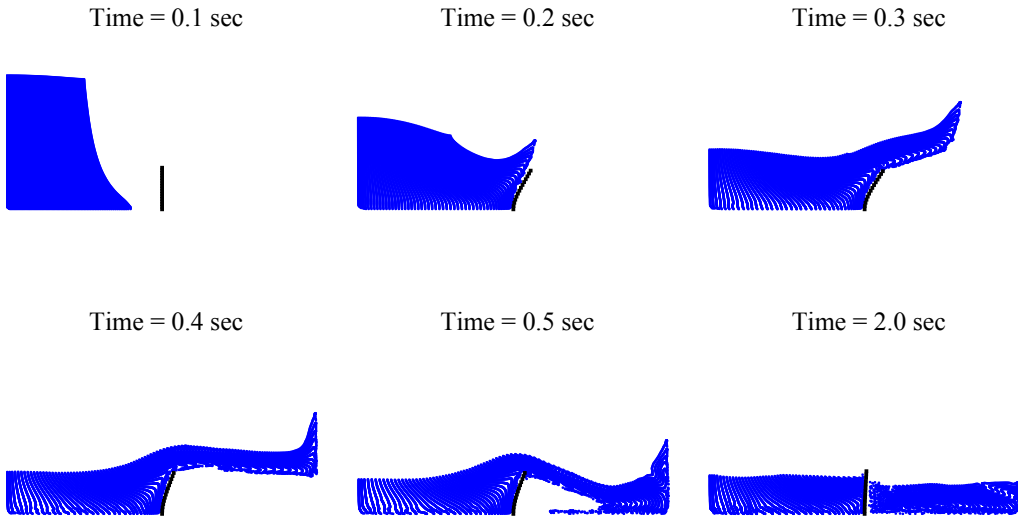


Figure 3.6: Snapshots of a dam break as an elastic obstacle with background mesh.

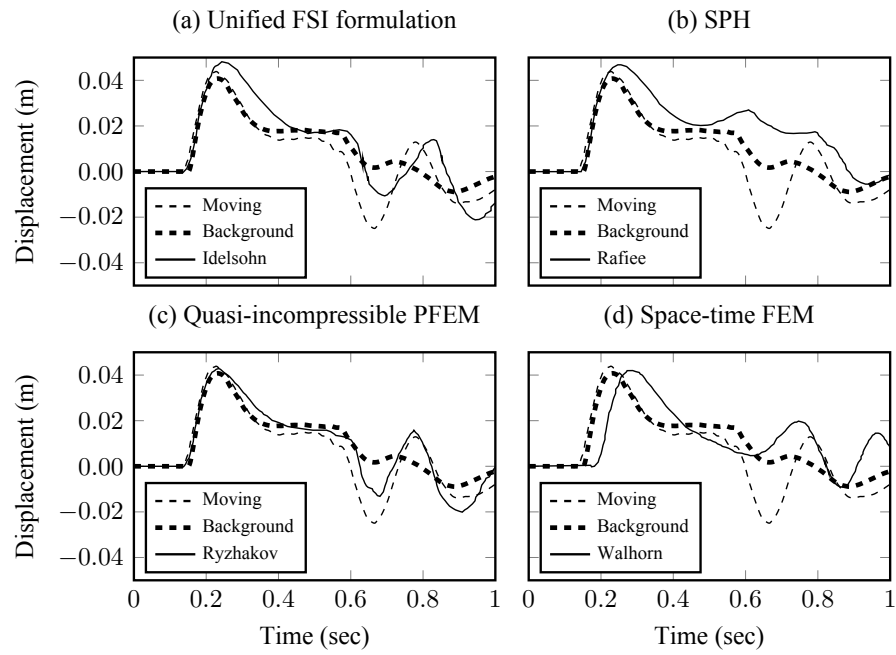


Figure 3.7: Comparison of the displacements of the free end of the elastic obstacle with different numerical approaches.

Comparisons of the time history of horizontal tip displacement of the obstacle by simulations by the aforementioned researchers are shown in Figure 3.7 along with the numerical method used by each researcher. The results of the moving mesh agree well with two previous PFEM formulations presented by Ryzhakov et al. (2010; and Idelsohn et al. (2008), as shown in Figure 3.7(a) and (c), and the background mesh results are closer using the SPH and space-time PFEM (Rafiee and Thiagarajan 2009; Walhorn et al. 2005); see Figure 3.7(b) and (d).

3.3.2 Dam break presented as a nonlinear material obstacle

One of the advantages of implementing the FSI in OpenSees is that it utilizes the libraries of nonlinear materials available in the framework. To demonstrate the ability of the FSI implementation to simulate the interaction between a fluid and a structure responding in the nonlinear material range, the same model is used with the obstacle composed of a co-rotational mesh of displacement-based elements. Two Gauss points are used in each element where cross sections are discretized by ten fibers, each with the uniaxial bilinear steel stress-strain response shown in Figure 3.8(a).

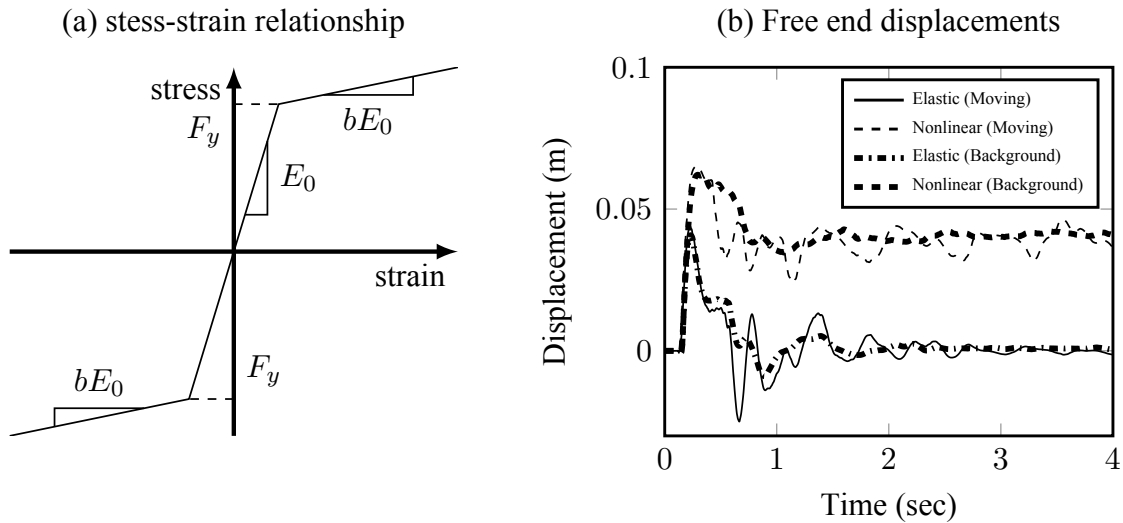


Figure 3.8: Nonlinear material for obstacle in dam-break problem and comparison of free-end displacements with elastic material.

The stress strain behavior is characterized by parameters of yield strength $F_y = 5 \times 10^6$ Pa, an initial elastic tangent $E_0 = 10^6$ Pa, and a strain hardening ratio $b = 0.02$. As a way of demonstrating the effects of nonlinear material response for the obstacle, the initial elastic tangent is the same as that shown in the previous example. The comparison of tip deflections for elastic and nonlinear materials using moving and background mesh are shown in Figure 3.8(b). The nonlinear material has residual displacements at the steady

state, indicating damage to the obstacle.

3.3.3 A 2D sloshing example with unified FSM

The incompressible FSM works well for inviscid and near-inviscid flows. For large viscosity fluid, the unified FSM must be used. In this example, the unified FSM is compared with the incompressible FSM for fluids of different viscosities [adapted from Oñate et al. (2014) with modifications of the tank dimensions and tank walls].

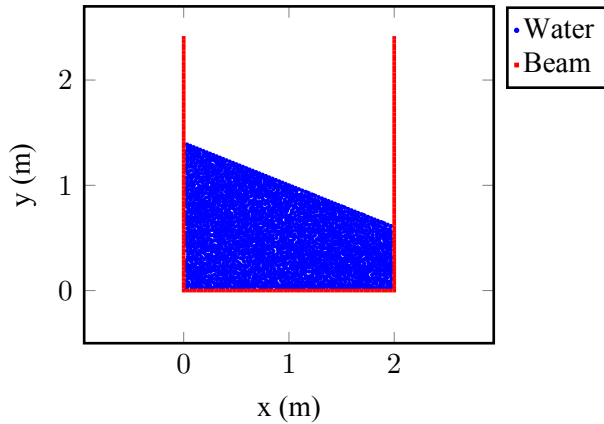


Figure 3.9: Model of 2D water sloshing analysis in a rectangular tank.

As shown in Figure 3.9, the width and height of the tank are 2 m and 2.4 m, respectively. The initial water levels are set to 1.4 m and 0.6 m. The bulk modulus of the fluid is $\kappa = 2.15 \times 10^9$ Pa, and the fluid density is $\rho = 10^3$ kg/m³. The out-of-plane thickness of the fluid elements is assumed to be 0.1 m.

The walls of the tank are made up of flexible beam–column finite elements with material and geometric nonlinearity. The walls are discretized in to a co-rotational mesh of beam elements with a cross section of 0.5 m by 0.5 m discretized by fibers, each with the uniaxial bilinear stress–strain relationship in Figure 3.8(a). The stress–strain behavior is characterized by the initial elastic stiffness $E_0 = 10^6$ Pa, yield strength $F_y = 4 \times 10^3$ Pa, and strain hardening ratio $b = 0.02$. The density of the structure is set to $\rho_s = 100$ kg/m³. The walls are fixed against deflection and rotation at both bottom corners of the tank.

The unified FSM and incompressible FSM are run using viscosity $\mu = 10^{-3}$ Pa·s and time step $\Delta t = 10^{-3}$ sec; snapshots of the simulation are shown in Figure 3.10. Flexural yielding initiates at the left end of the bottom beam, followed by yielding at the right end and middle of the beam. Note the subsequent large nonlinear deformation of the beam in Figure 3.10 after $t = 0.2$ sec. Since the viscosity is small, neither divergence nor slow convergence is found in all time steps for both methods. The tip deflections of the left and right columns and the middle deflection of the bottom beam using both methods match; see

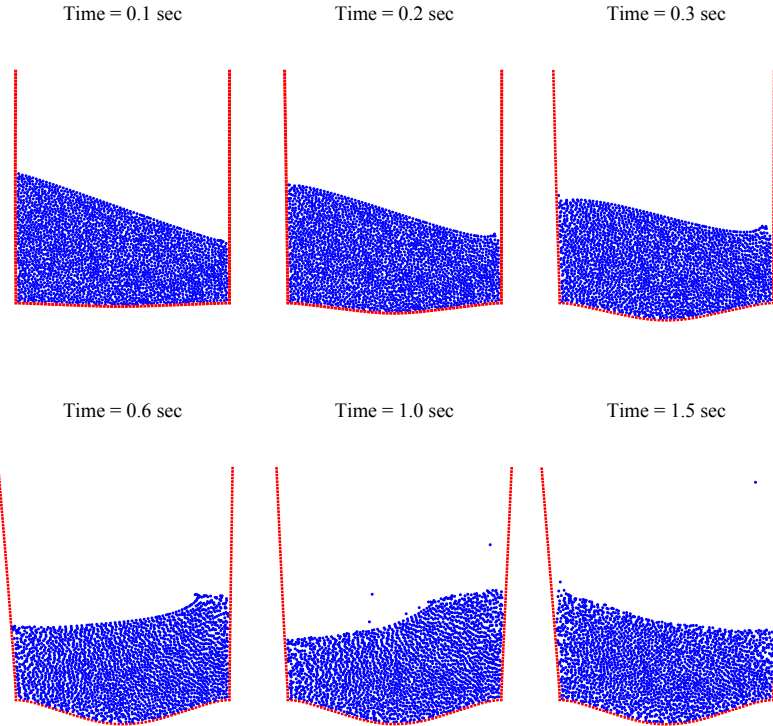


Figure 3.10: Snapshots of water sloshing in a flexible tank using the unified FSM and the incompressible FSM with viscosity $\mu = 10^{-3}$ Pa-s and $\Delta t = 10^{-3}$ sec.

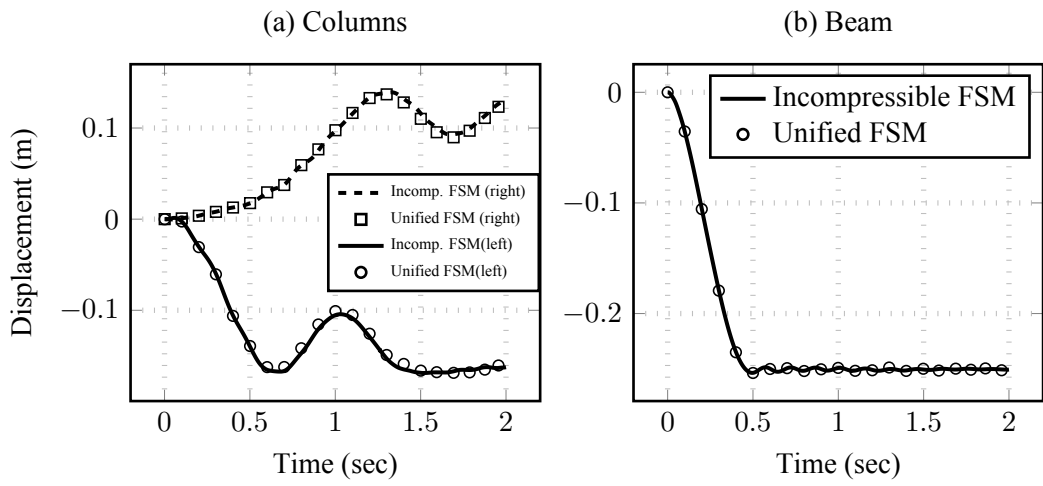


Figure 3.11: Tip deflection of left and right columns and middle deflection of the bottom beam using the unified FSM and the incompressible FSM with viscosity $\mu = 10^{-3}$ Pa-s and $\Delta t = 10^{-3}$ sec.

Figure 3.11. The columns undergo damped vibration after about 1.0 sec into the simulation, while the beam quickly reaches a static solution at about 0.5 sec due to the weight of the fluid supporting it. This case establishes that neither the unified nor incompressible FSM show convergence difficulties in simulating FSI with fluids of low viscosity.

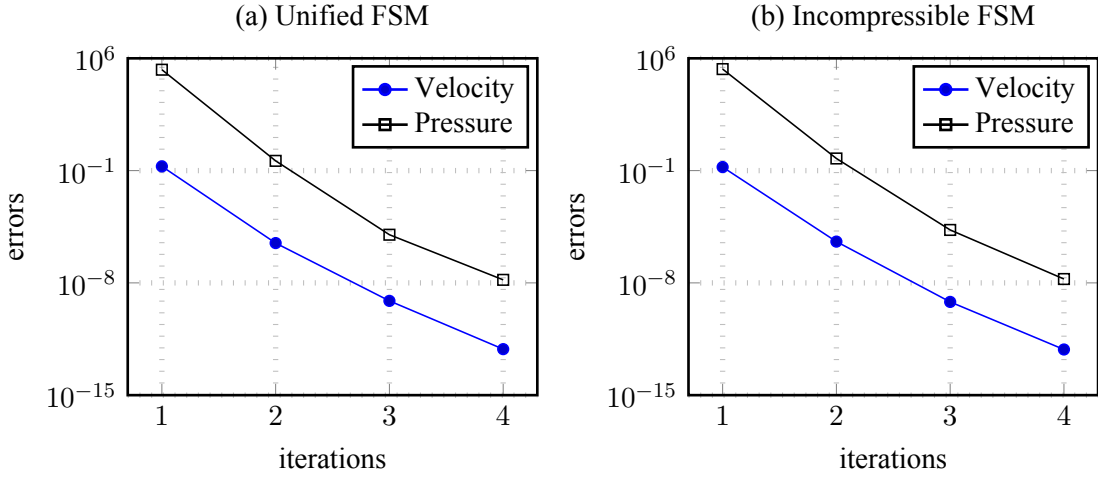


Figure 3.12: Convergence of velocity and pressure using unified FSM and incompressible FSM with viscosity $\mu = 10^{-3}$ Pa-s and time step $\Delta t = 10^{-3}$ sec.

Table 3.1: Iterations to achieve convergence for different viscosity with $\Delta t = 10^{-3}$ sec.

Viscosity, μ (Pa-s)	Unified FSM	Incompressible FSM
0.001	4	4
1.0	4	5
50.0	4	68
10^3	4	does not converge
10^4	4	does not converge

To compare the efficiency of the unified versus the incompressible FSMs, the number of iterations required for convergence is shown using various values of viscosity. The convergence criterion is set in increments of velocity and pressure to be $|\delta v| \leq 10^{-6}$ m/sec and $|\delta p| \leq 10^{-6}$ Pa. In the following comparison, a single time step $\Delta t = 10^{-3}$ sec is run for five values of viscosity, and the convergence rates for both methods are compared. As shown in Figure 3.12–Figure 3.16, the fluid viscosity is increased over the range $\mu = 10^{-3}$ Pa-s ($Re = 10^6$), 1.0 Pa-s ($Re = 1400$), 50.0 Pa-s ($Re = 28$), 10^3 Pa-s ($Re = 0.7$), and 10^4 Pa-s ($Re = 0.042$). The number of iterations for the incompressible method increases from 4 to 68 for the first three values of viscosity, and failed to converge for the two largest

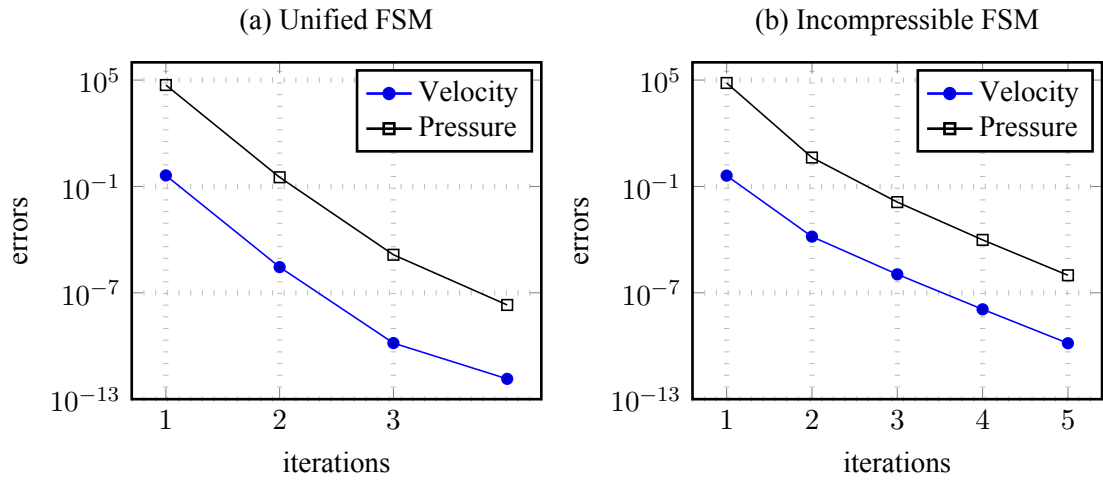


Figure 3.13: Convergence of velocity and pressure using unified FSM and incompressible FSM with viscosity $\mu = 1.0 \text{ Pa-s}$ and time step $\Delta t = 10^{-3} \text{ sec}$.

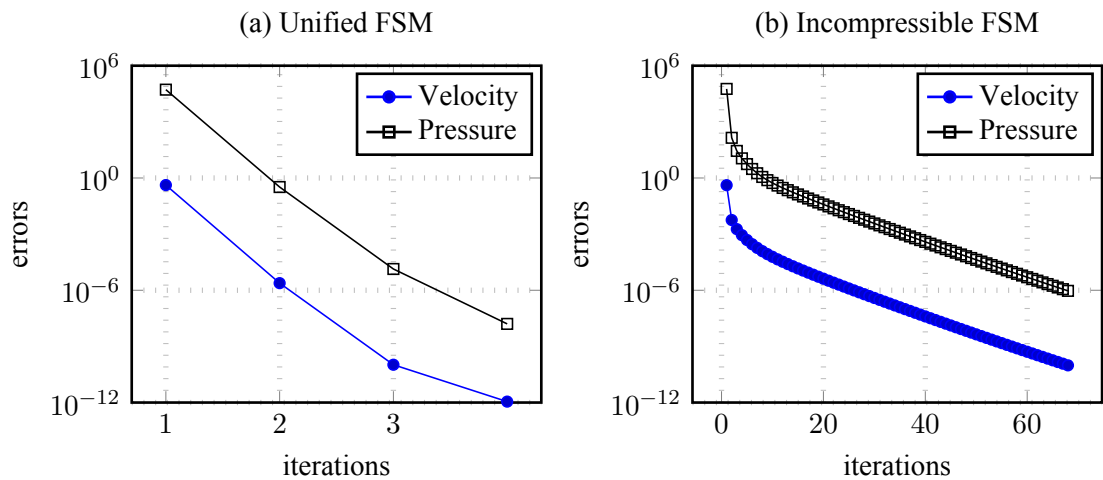


Figure 3.14: Convergence of velocity and pressure using unified FSM and incompressible FSM with viscosity $\mu = 50 \text{ Pa-s}$ and time step $\Delta t = 10^{-3} \text{ sec}$.

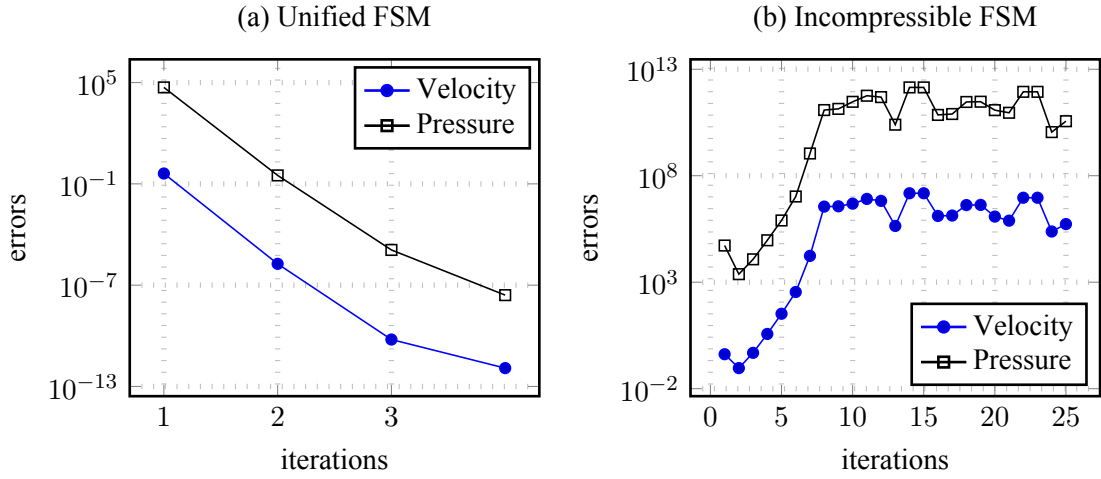


Figure 3.15: Convergence of velocity and pressure using unified FSM and incompressible FSM with viscosity $\mu = 10^3$ Pa-s and time step $\Delta t = 10^{-3}$ sec.

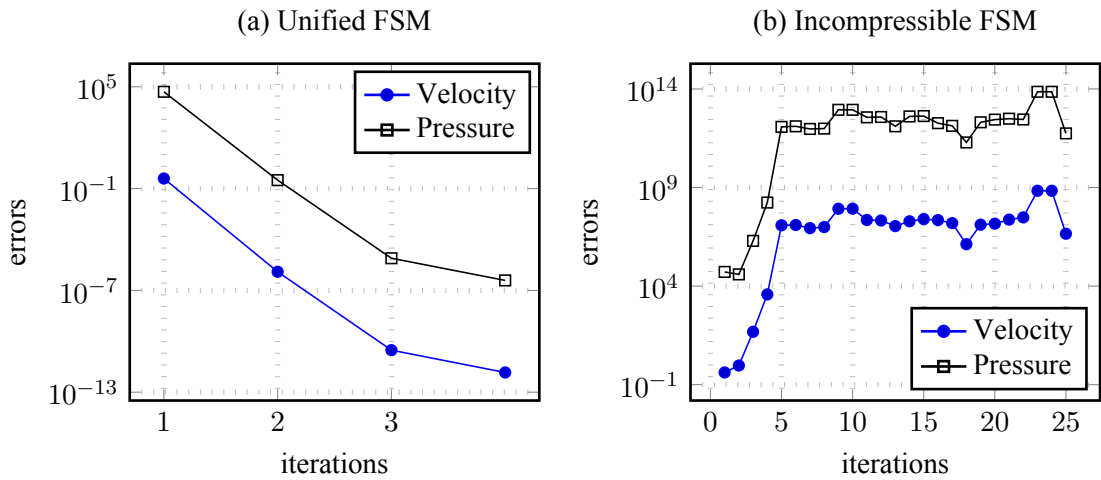


Figure 3.16: Convergence of velocity and pressure using unified FSM and incompressible FSM with viscosity $\mu = 10^4$ Pa-s and time step $\Delta t = 10^{-3}$ sec.

values of viscosity. On the other hand, the unified method converges in four iterations for all values of viscosity. Comparisons of the number of iterations required for different values of viscosity are summarized in Table 3.1. As the viscosity increases, so does the number of iterations for the incompressible FSM. In contrast, the number of iterations of the unified FSM is basically constant and independent of viscosity.

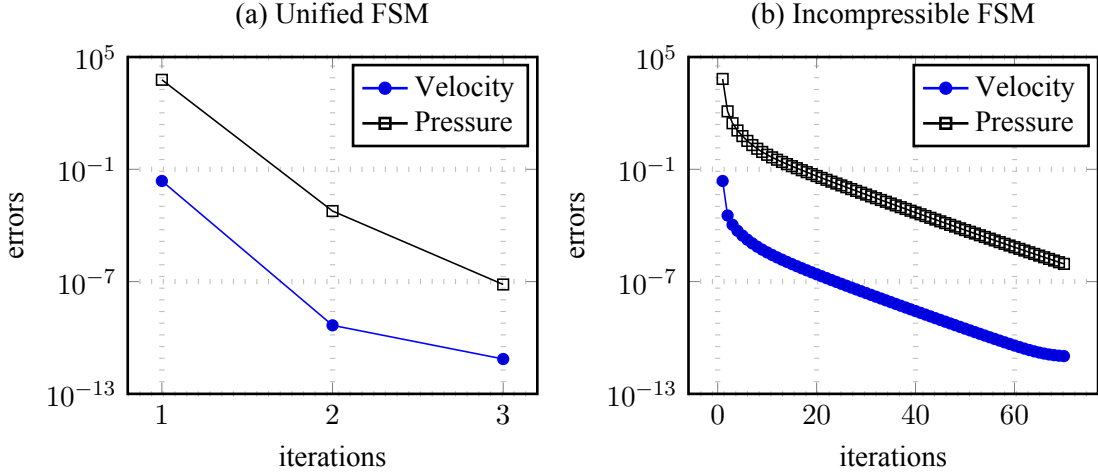


Figure 3.17: Convergence of velocity and pressure using unified FSM and incompressible with viscosity $\mu = 10^3$ Pa-s and time step $\Delta t = 5 \times 10^{-5}$ sec.

Table 3.2: Number of iterations required to achieve convergence for different viscosity with $\Delta t = 5 \times 10^{-5}$ sec.

Viscosity, μ (Pa-s)	Unified FSM	Incompressible FSM
10^{-3}	3	3
10^0	3	4
0.5×10^2	3	7
10^3	3	70
10^4	3	does not converge

A decreased time-step size improves the convergence of velocity and pressure. When the viscosity is fixed at $\mu = 10^3$ Pa-s but the time step Δt decreases from 10^{-3} sec to 5×10^{-5} sec, the incompressible method is able to converge in 70 iterations; see Figure 3.17. The improved convergence rate for a decreasing time step is also observed when the viscosity is fixed at a very high value $\mu = 10^4$ Pa-s. The time steps $\Delta t = 10^{-3}$ sec (Figure 3.16) and $\Delta t = 5 \times 10^{-5}$ sec (Figure 3.18) fail, and only the time step $\Delta t = 4 \times 10^{-6}$ sec (Figure 3.19) reaches convergence in 56 iterations for the incompressible method. Although a decreasing time step helps with convergence, it increases the simulation cost

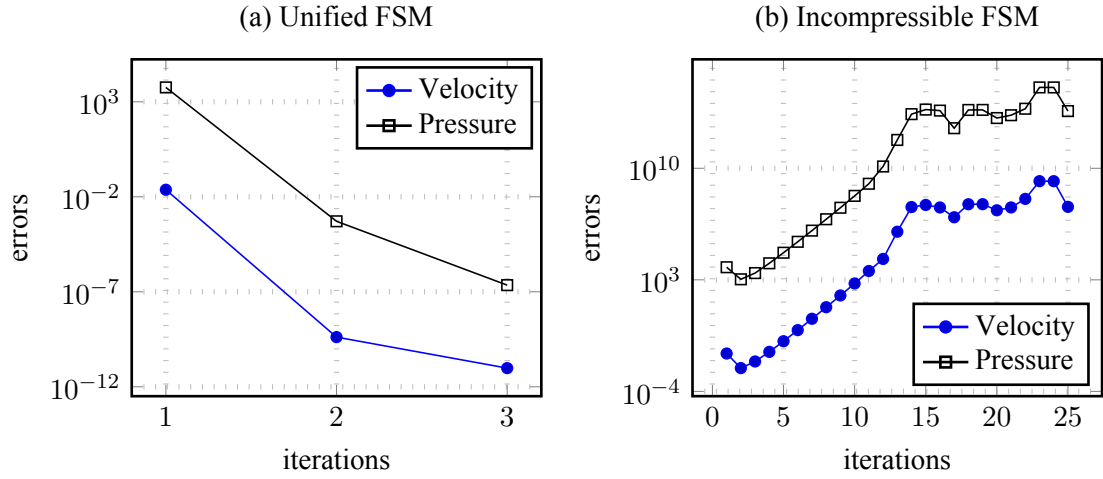


Figure 3.18: Convergence of velocity and pressure using unified FSM and incompressible FSM with viscosity $\mu = 10^4$ Pa-s and time step $\Delta t = 5 \times 10^{-5}$ sec.

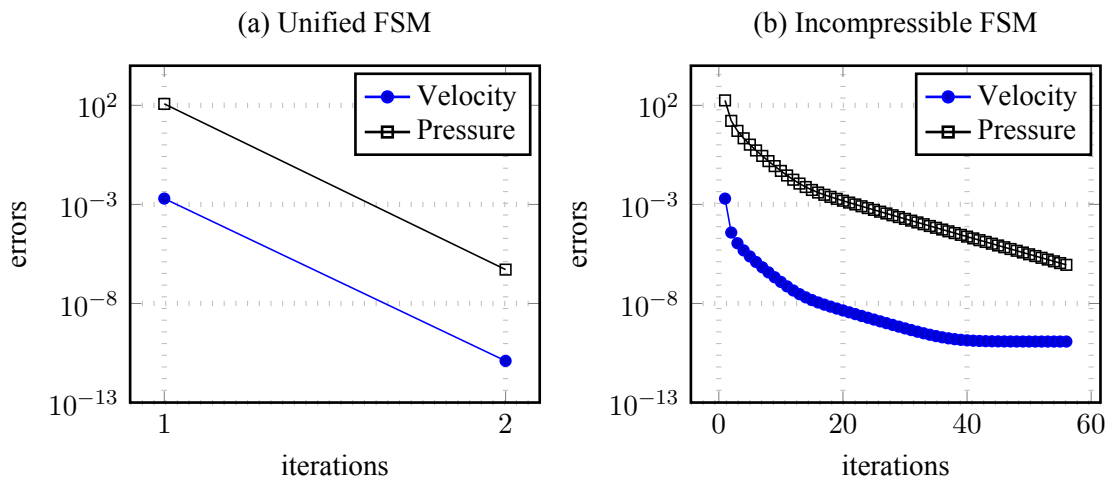


Figure 3.19: Convergence of velocity and pressure using unified FSM and incompressible FSM with viscosity $\mu = 10^4$ Pa-s and time step $\Delta t = 4 \times 10^{-6}$ sec.

Table 3.3: Number of iterations required to achieve convergence for different viscosity with $\Delta t = 4 \times 10^{-6}$ sec.

Viscosity, μ (Pa-s)	Unified FSM	Incompressible FSM
10^{-3}	2	2
10^0	2	3
0.5×10^2	2	4
10^3	2	7
10^4	2	56

significantly for the incompressible method, whereas convergence is achieved in the same small number of iterations using the unified method, demonstrating its capability of efficient simulation of a highly viscous flow. Comparisons of the number of iterations for different values of viscosity and time steps computed by the two methods are also summarized in Tables 3.2 and 3.3 to show the dependence of the incompressible method on fluid viscosity and time step size, versus the independence of the unified method on these factors.

4 Python Scripting in OpenSees

To allow users to take advantage of programming constructs such as conditionals, iterations, and procedures, OpenSees extends the interpreter of *Tcl* with commands for model building and analysis. Although *Tcl* is very flexible and has many strengths in string processing, it is not well-suited to scientific computing applications. *Tcl*'s use of strings as the only native data type and the resulting cumbersome syntax for mathematical expressions create a steep learning curve for users of OpenSees, many of whom learned MATLAB or Python as undergraduate engineering students.

Python is general-purpose programming language that contains a large ecosystem of libraries; it has been adopted by the scientific community as a “glue” language for many applications. With its extension to Python, users of OpenSees may now gain access to the plotting library Matplotlib, numerical libraries Numpy, and Scipy, interactive server Jupyter, 3D visualization library Mayavi, statistics library pandas, and web development library Flask, among others. In addition, OpenSees can now use the Visualization Toolkit (VTK), an open-source, permissively licensed, cross-platform toolkit for scientific data processing, visualization, and data analysis, as one of its post-processing tools. Therefore, the OpenSeesPy is created as an implementation of the Python interpreter for use with OpenSees. The underlying framework is general and can easily accommodate other scripting languages such as Ruby, Julia, and R.

4.1 Implementation of Python Interpreter

As shown in Figure 3.1, the model components in the domain and analysis options are set by user scripts. For the *Tcl* interpreter, the user scripts will invoke *Tcl* commands to create the finite-element model. For example, a *Tcl* `node` command will create a Node object from user input in the *Tcl* API (Welch 2000), such as `Tcl_GetDouble`. Likewise, to implement the Python interpreter, internal OpenSees objects must link to Python commands. Since much of the code for reading input, creating finite-element domain objects, performing analyses, and recording results are duplicated among interpreters, the implementation of Python utilizes a core, interpreter-independent OpenSees API that populates the domain and performs analyses, as shown in Figure 4.1.

The core APIs are separated from any interpreters and collected in a class to populate

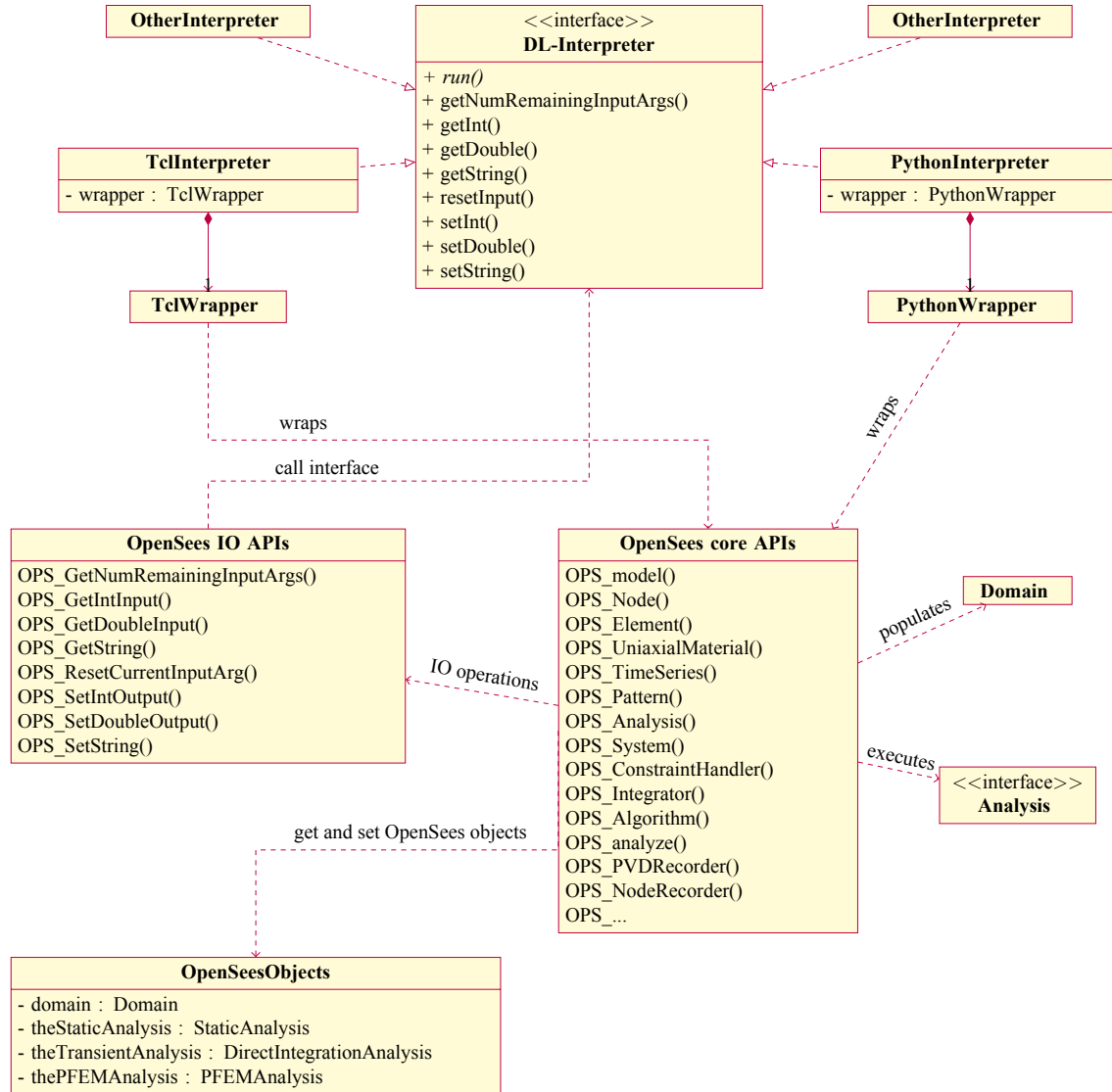


Figure 4.1: Class diagram of multi-interpreter interface.

domain components and to execute analysis. The interaction of core APIs with specific interpreters is done through the IO APIs. There are eight basic input/output functions for obtaining integer, floating point, and string inputs. Each scripting language will define its own interpreter class that implements the DL_Interpreter interface, for the eight IO APIs. If an IO operation is required, a core API will call the OpenSees IO APIs, e.g., OPS_GetIntInput, which are also interpreter-independent and will make polymorphic calls to the eight basic IO functions through the DL_Interpreter interface. With this design, the core OpenSees APIs are completely separated from the interpreter, and the effort to add a new interpreter is minimized.

```
int PythonInterpreter::getDouble(double *data, int numArgs) {
    int curr = wrapper.getCurrentArg();
    if (wrapper.getNumberArgs() - curr < numArgs) return -1;
    for (int i=0; i<numArgs; i++) {
        if (!PyFloat_Check(o)) return -1;
        PyObject *o = PyTuple_GetItem(wrapper.getCurrentArgv(), curr);
        wrapper.incrCurrentArg();
        data[i] = PyFloat_AS_DOUBLE(o);
    }
    return 0;
}
```

Figure 4.2: The implementation of getDouble in Python interpreter.

```
int TclInterpreter::getDouble(double *data, int numArgs) {
    int curr = wrapper.getCurrentArg();
    const char* argv = wrapper.getCurrentArgv();
    if (wrapper.getNumberArgs() - curr < numArgs) return -1;
    for (int i=0; i<numArgs; i++) {
        if (Tcl_GetDouble(interp, argv[curr], &data[i]) != TCL_OK) {
            wrapper.incrCurrentArg();
            return -1;
        } else wrapper.incrCurrentArg();
    }
    return 0;
}
```

Figure 4.3: The implementation of getDouble in *Tcl* interpreter.

As an example of IO API, the implementation of the virtual function getDouble is inherited by Python and *Tcl* interpreters shown in Figures 4.2 and 4.3. As can be seen,

```

int OPS_Node()
{
    Domain* theDomain = OPS_GetDomain();
    int ndm = OPS_GetNDM();
    int ndf = OPS_GetNDF();

    // get tag
    int tag = 0;
    int numData = 1;
    if(OPS.GetIntInput(&numData, &tag) < 0) {
        opserr<<"WARNING tag is not integer\n";
        return -1;
    }

    // get crds
    Vector crds(ndm);
    if(OPS_GetDoubleInput(&ndm, &crds(0)) < 0) {
        opserr<<"WARNING node coord are not double\n";
        return -1;
    }

    // create node
    Node* theNode = 0;
    if(ndm == 1) {
        theNode = new Node(tag,ndf,crds(0));
    } else if(ndm == 2) {
        theNode = new Node(tag,ndf,crds(0),crds(1));
    } else {
        theNode = new Node(tag,ndf,crds(0),crds(1),crds(2));
    }

    // add node to domain
    if(theDomain->addNode(theNode) == false) {
        opserr<<"WARNING: failed to add node to domain\n";
        delete theNode;
        return -1;
    }

    return 0;
}

```

Figure 4.4: The implementation of the core API OPS_Node.

the Python interpreter assigns a double number through the `PyFloat_AS_DOUBLE` function and the *Tcl* interpreter through the `Tcl_GetDouble` function. The polymorphic feature of C++ will find the correct implementation depending on the calling interpreter.

To demonstrate the implementation of core APIs, the definition of the API `OPS_Node` is shown in Figure 4.4. The `OPS_Node` API calls the IO APIs to obtain the input parameters of nodal tag and coordinates without knowing the calling interpreter. A Node object is then created and added to the domain. The API returns to zero when marking a successful operation but will return negative values if something is wrong with the inputs and operations.

4.2 Illustrative Examples

4.2.1 Nonlinear truss example

For new users and users who are familiar with *Tcl*, this example shows the simplicity of Python scripting and its similarity to its *Tcl* counterpart.

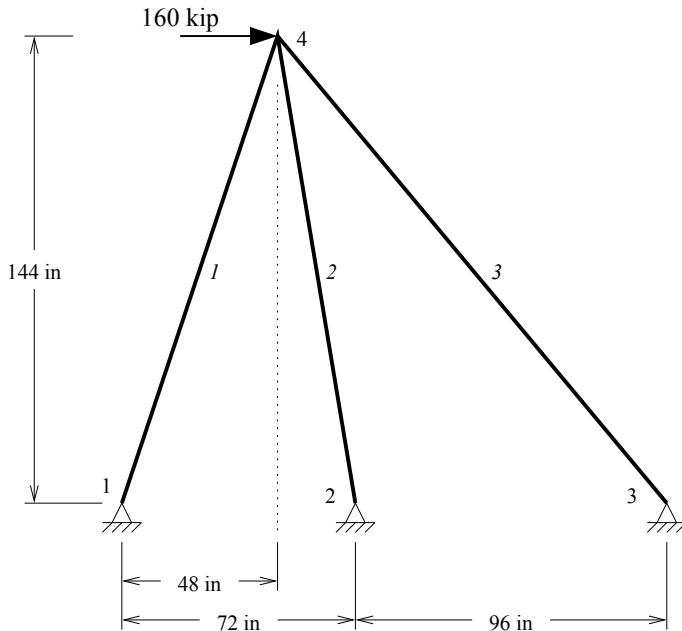


Figure 4.5: Truss model for the Python interpreter.

In the truss model shown in Figure 4.5, nodes are numbered from one through four and elements one through three. Snippets of Python code to create the truss model are shown in Figure 4.6. For OpenSees *Tcl* users, the Python functions, such as `wipe`, `model`, `node`, `fix`, etc., are identical to *Tcl* commands with Python syntax; however, the concise syntax

```

from opensees import *

wipe() # remove existing model
model('basic', '-ndm', 2, '-ndf', 2) # create model

x = [0.0, 72.0, 168.0, 48.0]
y = [0.0, 0.0, 0.0, 144.0]
for i in range(4):
    node(i+1, x[i], y[i]) # create nodes
    if i<3:
        fix(i+1, 1, 1) # boundary conditions

A = 4.0; E = 29000.0; # create material
alpha = 0.05; sigmaY = 36.0
uniaxialMaterial('Hardening', 1, E, sigmaY, 0.0, alpha/(1-alpha)*E)

for i in range(3):
    element('Truss',i+1,i+1,4,A,1) # create truss elements

timeSeries('Linear', 1) # create TimeSeries
pattern('Plain', 1, 1) # create a plain load pattern
load(4, 160.0, 0.0) # Create the nodal load

Nsteps = 1000
system("ProfileSPD") # set analysis options
numberer("RCM")
constraints("Plain")
integrator("LoadControl", 1.0/Nsteps)
algorithm("Newton")
test('NormUnbalance', 1e-8, 10)
analysis("Static")

for i in range(Nsteps):
    analyze(1) # perform the analysis

```

Figure 4.6: Python scripts for nonlinear material truss analysis.

of Python `for` loop, math expressions and variable assignments make the code much easier to read and understand than *Tcl*.

Here, all functions in the OpenSees module are imported to Python. A better practice is to import OpenSees with a short name as `import opensees as ops`. Then the calls to OpenSees functions require a dot scoping operator in the module, as shown in Figure 4.7.

```
import opensees as ops
ops.wipe()
ops.model('basic', '-ndm', 2, '-ndf', 2)
```

Figure 4.7: Python scripts for importing OpenSeesPy module.

With the Python libraries NumPy and Matplotlib, the analysis results can be plotted directly from the Python scripts (Figure 4.8).

```
import numpy as np
import matplotlib.pyplot as plt

data = np.zeros((Nsteps+1,2)) # data array
for j in range(Nsteps):
    analyze(1)
    data[j+1,0] = nodeDisp(4,1)      # save disp
    data[j+1,1] = getLoadFactor(1)*160 # save load factor

plt.plot(data[:,0], data[:,1])      # plotting
plt.xlabel('Horizontal Displacement')
plt.ylabel('Horizontal Load')
plt.show()
```

Figure 4.8: Python scripts for plotting.

The variable `data` in Figure 4.8 is a NumPy array, which stores the nodal displacement and load factor. The plotting is shown in the Figure 4.9.

4.2.2 Dam break problem as a nonlinear material obstacle example

The numerical example shown in Section 3.3.2 is used here to illustrate the scripting of the fluid–structure interaction simulation. The FSI commands can be added to any existing scripts for structural analysis. To add the fluid model, if the background mesh method is used, a group of particles are added as in Figure 4.10.

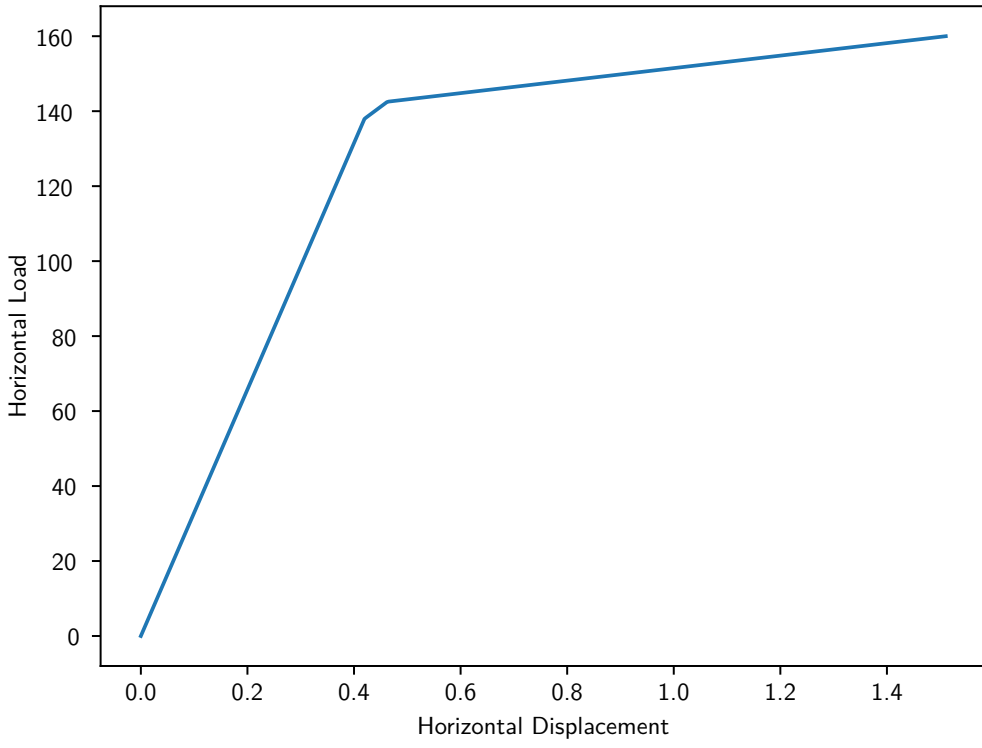


Figure 4.9: Python plotting for the nonlinear truss example.

These particles represent the water column in Figure 3.4. Then, a structural model for a nonlinear material obstacle is created in Figure 4.11. No elements are explicitly created in this code since the `dispBeamColumn` elements are internally constructed in the `mesh` command.

```

eleArgs = ['PFEMElementBubble', rho, mu, b1, b2, thk, kappa]
partArgs = ['quad', 0.0, 0.0, L, 0.0, L, H, 0.0, H, nx, ny]
parttag = 1
mesh('part', parttag, *partArgs, *eleArgs, '-vel', 0.0, 0.0)

```

Figure 4.10: Python code for adding fluid particles for the background mesh method.

After the structural model is created, the background mesh is defined with one line of code in Figure 4.12, where `lower` and `upper` defines the range of the background mesh, and `wNodes` and `sNodes` notifies the background mesh wall nodes and structural nodes. The codes in Figures 4.10 and 4.12 show typical FSI commands, and how simple it is to

```

node(1, 0.0, 0.0); node(2, 4*L, 0.0) # structural and wall nodes
node(3, 0.0, H); node(4, 4*L, H)
node(5, 2*L, 0.0); node(6, 2*L, Hb)

mesh('line', linetag, 5, 3,1,5,2,4, id, ndf, h) # mesh of walls

fixedNodes = getNodeTags('-mesh', linetag) # fix walls
for nd in fixedNodes:
    fix(nd,1,1,1)

geomTransf('Corotational', transfTag) # transformation

# mesh of the obstacle
uniaxialMaterial('Steel01',matTag,Fy,E0,hardening)
section('Fiber',secTag)
patch('rect', matTag, numfiber, numfiber, 0.0, 0.0, thk, thk)
beamIntegration( 'Legendre', inteTag, secTag, numpts)
eleArgs = ['dispBeamColumn',transfTag,inteTag]
mesh('line', coltag, 2, 5,6, id, ndf, 0.5*h, *eleArgs)

```

Figure 4.11: Python code for a nonlinear material obstacle.

```

mesh('bg', h, *lower, *upper, '-structure',len(wNodes),*wNodes,
      '-structure',len(sNodes),*sNodes)

```

Figure 4.12: Python script for defining the background mesh.

include the FSI in existing structural models. Finally, the analysis for the FSI simulation is straightforward and is performed as that for regular structural analysis (Figure 4.13).

The FSI analysis implements its own `test`, `integrator`, `system`, and `analysis` objects. The `analyze` command now accepts no parameters, which performs an analysis with time step `dtmax`. If the current time step fails, the `analyze` command will reduce the step size and run the analysis again until a successful analysis is performed or the minimum time step size is achieved. The results of the FSI analysis are shown in Figure 3.8.

```

constraints('Plain') # create constraint object
numberer('Plain') # create numberer object
test('PFEM', 1e-5, 1e-5, 1e-5, 1e-5, 1e-5, 1e-5, 100, 3, 1, 2)
algorithm('Newton') # create algorithm object
integrator('PFEM')# create integrator object
system('PFEM') # create SOE object
analysis('PFEM', dtmax, dtmin, b2) # create analysis object

while getTime() < totaltime:
    if analyze() < 0:
        break
    remesh()

```

Figure 4.13: Python code for running FSI analysis.

4.3 Python Commands Manual

The latest manual has been published online at <https://openseespydoc.readthedocs.io/en/latest/>. The manual includes all existing commands, installation information, and additional examples. New versions of OpenSeesPy will be updated on this web page, as well as providing new commands and examples.

4.4 Python and *Tcl* Tests

To validate the OpenSeesPy implementation, many models were tested against analytic and numerical results from OpenSees *Tcl* and other software. A benchmark is shown here for seventeen models, from which the exact same results are generated for both Python and *Tcl*. Both scripts are timed and shown in Table 4.1 where the Python implementation

Table 4.1: Timing of Python and *Tcl* scripts for same models.

	OpenSeesPy	OpenSeesTcl	Speedup of Python
Time	131.8 sec	207.5 sec	1.57

is 1.57 times faster than the *Tcl* version for the same models and analyses. The Python and *Tcl* scripts for testing are shown in Figures 4.14 and 4.15, respectively. Both Python and *Tcl* scripts generated the same results and have been verified by exact numerical solutions.

```

# Python script to run all the verification scripts

import os
import sys
from opensees import *

exec(open('Truss.py','r').read())
exec(open('MomentCurvature.py','r').read())
exec(open('RCFramePushover.py','r').read())
exec(open('ElasticFrame.py','r').read())
exec(open('DynAnal_BeamWithQuadElements.py','r').read())
exec(open('Ex1a.Canti2D.EQ.modif.py','r').read())
exec(open('EigenAnal_twoStoreyShearFrame7.py','r').read())
exec(open('EigenAnal_twoStoreyFrame1.py','r').read())
exec(open('sdofTransient.py','r').read())
exec(open('PlanarTruss.py','r').read())
exec(open('PlanarTruss.Extra.py','r').read())
exec(open('PortalFrame2d.py','r').read())
exec(open('EigenFrame.py','r').read())
exec(open('EigenFrame.Extra.py','r').read())
exec(open('AISC25.py','r').read())
exec(open('PlanarShearWall.py','r').read())
exec(open('PinchedCylinder.py','r').read())

print("====")
print("Done with testing examples.")
print("====")

```

Figure 4.14: Python code for testing.

```

# script to run all the verification scripts

source Truss.tcl
source MomentCurvature.tcl
source RCFramePushover.tcl
source ElasticFrame.tcl
source DynAnal_BeamWithQuadElements.tcl
source Ex1a.Canti2D.EQ.modif.tcl
source EigenAnal_twoStoreyShearFrame7.tcl
source EigenAnal_twoStoreyFrame1.tcl
source sdofTransient.tcl
source PlanarTruss.tcl
source PlanarTruss.Extra.tcl
source PortalFrame2d.tcl
source EigenFrame.tcl
source EigenFrame.Extra.tcl
source AISC25.tcl
source PlanarShearWall.tcl
source PinchedCylinder.tcl

puts =====
puts "Done with testing examples."
puts =====

```

Figure 4.15: *Tcl* code for testing.

As shown in Table 4.2, an undamped system harmonic excitation is tested for 1000 time steps by computing the solution and checking the results against exact solution with Chopra (2007) (Section 3.1). The results shown are for the last step at 11.255 sec.

Table 4.2: Verification of elastic SDOF systems of Python and *Tcl* with Chopra (2007) (Section 3.1).

OpenSeesPy	OpenSeesTcl	Exact
0.9574599250636698	0.95746	0.9574597093660693

The comparison of earthquake responses for various periods and damping ratios between Python, *Tcl*, and the exact solutions are shown in Table 4.3.

Table 4.3: Verification of elastic SDOF systems of Python and *Tcl* with Chopra (2007) (Section 6.4).

Period	dampRatio	OpenSeesPy	OpenSeesTcl	Exact
0.50	0.02	2.69	2.69	2.67
1.00	0.02	5.96	5.96	5.97
2.00	0.02	7.48	7.48	7.47
2.00	0.00	9.92	9.92	9.91
2.00	0.02	7.48	7.48	7.47
2.00	0.05	5.38	5.38	5.37

The results of period and displacement from the static pushover analysis are shown in Tables 4.4 and 4.5, respectively, for a 2D elastic frame compared with SAP2000 and SeismoStruct.

Table 4.4: Verification of period for 2D Elastic Frame with SAP2000 and SeismoStruct.

Period	OpenSeesPy	OpenSeesTcl	SAP2000	SeismoStruct
1	1.27321	1.27321	1.2732	1.2732
2	0.43128	0.43128	0.4313	0.4313
3	0.24204	0.24204	0.2420	0.2420
4	0.16018	0.16018	0.1602	0.1602
5	0.11899	0.11899	0.1190	0.1190
6	0.09506	0.09506	0.0951	0.0951
7	0.07951	0.07951	0.0795	0.0795

Table 4.5: Verification of displacement for 2D Elastic Frame with SAP2000 and SeismoStruct.

Displacement	OpenSeesPy	OpenSeesTcl	SAP2000	SeismoStruct
Top	1.451	1.451	1.45	1.45
Axial Force Bottom Left	69.987	69.987	69.99	70.01
Moment Bottom Left	2324.677	2324.677	2324.68	2324.71

The benchmark problem (Tables 4.6 and 4.7) is from the AISC Design Guide 25 (Kaehler et al. 2011) for frame design using web-tapered members. This is a nonlinear problem with single curvature. The comparison of tip displacements for different curvatures are shown in Table 4.6 against the exact solutions, and the base moments are compared in Table 4.7.

Table 4.6: Prismatic beam benchmark problems with Kaehler et al. (2011) (tip displacements).

numEle	alpha	Exact	OpenSeesPy	OpenSeesTcl	%Error
1	0.00	0.3957	0.3957	0.3957	-0.0
1	0.10	0.4391	0.4391	0.4391	-0.0
1	0.20	0.4933	0.4933	0.4933	-0.0
1	0.30	0.5630	0.5630	0.5630	-0.0
1	0.40	0.6560	0.6560	0.6560	-0.0
1	0.50	0.7860	0.7860	0.7860	-0.0
1	0.60	0.9811	0.9811	0.9811	-0.0
1	0.67	1.1879	1.1879	1.1879	-0.0

Table 4.7: Prismatic beam benchmark problems with Kaehler et al. (2011) (base moments).

numEle	alpha	Exact	OpenSeesPy	OpenSeesTcl	%Error
1	0.00	1960.00	1960.00	1960.00	0.0
1	0.10	2138.88	2138.88	2138.88	-0.0
1	0.20	2361.94	2361.94	2361.94	-0.0
1	0.30	2648.09	2648.09	2648.09	-0.0
1	0.40	3028.86	3028.86	3028.86	-0.0
1	0.50	3560.98	3560.98	3560.98	-0.0
1	0.60	4357.95	4357.95	4357.95	-0.0
1	0.67	5202.31	5202.31	5202.31	-0.0

The eigenvalue analysis for a large structure is compared with Bathe and Wilson (1972), SAP2000, and SeismoStruct in Table 4.8.

Table 4.8: Verification of eigenvalues of elastic frame with Bathe and Wilson (1972), SAP2000, and SeismoStruct.

OpenSeesPy	OpenSeesTcl	Bathe and Wilson (1972)	SAP2000	SeismoStruct
0.58954	0.5895	0.5895	0.5895	0.590
5.52696	5.5270	5.5270	5.5270	5.527
16.58787	16.5878	16.5879	16.5879	16.588

The analysis of a shear wall was compared with ETABS and SAP2000 in Table 4.9. A patch test was also done with different elements in OpenSees and compared with exact solutions for displacements under applied load Table 4.10.

Table 4.9: Verification of linear elastic planar shear wall with ETABS and SAP2000.

Stories	Height	Length	OpenSeesPy	OpenSeesTcl	ETABS	SAP2000	Diff.
6	720	120	2.3926	2.3926	2.4287	2.4293	0.0006
6	720	360	0.0985	0.0985	0.1031	0.1032	0.0001
6	720	720	0.0172	0.0172	0.0186	0.0187	0.0001
3	360	120	0.3068	0.3068	0.3205	0.3212	0.0007
3	360	360	0.0169	0.0169	0.0187	0.0187	0.0000
3	360	720	0.0046	0.0046	0.0052	0.0052	0.0000
1	120	120	0.0144	0.0144	0.0185	0.0187	0.0002
1	120	360	0.0024	0.0024	0.0029	0.0029	0.0000
1	120	720	0.0011	0.0011	0.0013	0.0013	0.0000

Table 4.10: Verification of shell elements with exact solutions.

Element Type	mesh	OpenSeesPy	OpenSeesTcl	Exact	%Error
ShellMITC4	4 x 4	-6.38579e-06	-6.38579e-06	-1.82489e-05	65.01
ShellMITC4	16 x 16	-1.68814e-05	-1.68814e-05	-1.82489e-05	7.49
ShellMITC4	32 x 32	-1.80250e-05	-1.80250e-05	-1.82489e-05	1.23
ShellDKGQ	4 x 4	-1.16624e-05	-1.16624e-05	-1.82489e-05	36.09
ShellDKGQ	16 x 16	-1.85314e-05	-1.85314e-05	-1.82489e-05	1.55
ShellDKGQ	32 x 32	-1.84395e-05	-1.84395e-05	-1.82489e-05	1.04
ShellNLDKGQ	4 x 4	-1.16624e-05	-1.16624e-05	-1.82489e-05	36.09
ShellNLDKGQ	16 x 16	-1.85314e-05	-1.85314e-05	-1.82489e-05	1.55
ShellNLDKGQ	32 x 32	-1.84395e-05	-1.84395e-05	-1.82489e-05	1.04

Additional results from Python and *Tcl* are shown in Figures 4.16 and 4.17, where the static, dynamic, and eigenvalue analyses are tested. By comparing the screen shots, the same results are obtained using both Python and *Tcl*.

```

=====
Starting Truss example
Passed!
=====
=====
Start MomentCurvature.py example
Estimated yield curvature:  0.000126984126984127
Passed!
=====
=====
Start RCFranePushover Example
=====
Starting RCFraneGravity example
Passed!
=====
Gravity Analysis Completed
Passed!
=====
=====
Start ElasticFrame example

Eqilibrium Check After Gravity:
SumX: Inputed: 0.0 + Computed: 0.0 =  0.0
SumY: Inputed: -3340.0 + Computed: 3340.000000000005 =  4.547473508864641e-13

Eqilibrium Check After Lateral Loads:
SumX: Inputed: 490.0 + Computed: -490.0 =  0.0
SumY: Inputed: -3340.0 + Computed: 3340.000000000005 =  4.547473508864641e-13

Eigenvalues:
T1 =  1.0401120938612853
T2 =  0.3526488583606463
T3 =  0.1930409642350476
T4 =  0.15628823050715795
T5 =  0.13080166151268388
Passed!
=====
=====
Start Simple supported beam modeled with 2D solid elements example
uy(9) = -0.39426414168933877
uy(9) = -0.007368472738064808
Passed!
=====
=====
Start cantilever 2D EQ ground motion with gravity example
u2 = -0.07441860465116278
Passed!
=====
=====
Start Eigen analysis of a two-storey shear frame
labmbda = 148.9197530705358
labmbda = 595.6790123329719
periods are [0.5148773207872785, 0.2574386603826558]
eigenvector 1: [0.499999999893345, 1.0]
eigenvector 2: [-1.0000000000213314, 1.0]
Passed!
=====
```

Figure 4.16: Part of benchmark results from Python.

```

=====
Starting Truss example
Passed!
=====
=====
Start MomentCurvature Example
Estimated yield curvature: 0.000126984126984127
Passed!
=====
=====
Start RCFramePushover Example
=====
Starting RCFrameGravity example
Passed!
=====
Gravity Analysis Completed
Passed!
=====
=====
Start ElasticFrame example

Eqilibrium Check After Gravity:
SumX: Inputed: 0.0 + Computed: 0.0 = 0.0
SumY: Inputed: -3340.0 + Computed: 3340.0000000000005 = 4.547473508864641e-13

Eqilibrium Check After Lateral Loads:
SumX: Inputed: 490.0 + Computed: -490.0 = 0.0
SumY: Inputed: -3340.0 + Computed: 3340.0000000000005 = 4.547473508864641e-13

Eigenvalues:
T1 = 1.0401120938612853
T2 = 0.3526488583606463
T3 = 0.1930409642350476
T4 = 0.15628823050715795
T5 = 0.13080166151268388
Passed!
=====
=====
Start Simple supported beam modeled with 2D solid elements example
uy(9) = -0.39426414168933876514
uy(9) = -0.00736847273806480810
Passed!
=====
=====
Start cantilever 2D EQ ground motion with gravity example
u2 = -0.07441860465116277579
Passed!
=====
=====
Start Eigen analysis of a two-storey shear frame
lambda = 148.91975307053579058447
lambda = 595.67901233297186536220
periods are 0.5148773207872785 0.2574386603826558
eigenvector 1: 0.499999999893345 1.0
eigenvector 2: -1.0000000000213314 1.0
Passed!
=====
```

Figure 4.17: Part of benchmark results from *Tcl*.

5 CONCLUSIONS

5.1 Summary and Conclusions

OpenSees finite-element software has been used in simulations of structures and soils to support various PEER research programs and performance-based earthquake engineering methodology; it has been applied to structural engineering, geotechnical engineering, earthquake engineering, and fire engineering. As PEER expands its tsunami research program, the ability to simulate tsunami and fluid–structure interaction (FSI), using the OpenSees framework is critical. This report has documented the development of a FSI module in OpenSees designed to support all existing and future structural elements and materials. The users do not need knowledge of computational fluid dynamics to run the FSI analysis. The fluid module can be easily added to existing scripts, and the underlying algorithm solutions, mesh updating, and time integration will be performed internally without interference from the user.

The open-source framework of the Python interpreter will keep OpenSees relevant to a large user base, with a structure that will easily support advances in scripting languages and nonlinear finite-element analysis. Since its publication in February 2018, the OpenSeesPy website has attracted more than ten thousand international visitors, from 289 locations in the U.S. and 1212 locations in 89 other countries. This shows the trend of using Python as the primary language for researchers in the OpenSees community. With the new capabilities of the FSI and Python, OpenSees can provide stronger support to both PEER researchers and international researchers as well.

5.2 Future Work

The FSI can be further improved by comparing it with additional experimental results of various incoming waves and their impact on different types of structures, and the results of such simulations used to develop design guidelines. Although the FSI module has used the PFEM primarily for coupling the structural and fluid domains, the PFEM can also be used for other problems, such as debris and moving objects interacting with structures, structural cracking, and corrosion. The OpenSeesPy has included response analysis, and in the future, the reliability analysis and parallel computing can be added in the Python interpreter.

Online documentation will be added with more examples and updated commands.

REFERENCES

- Arnold, D., Brezzi, F., and Fortin, M. (1984). “A stable finite element for the stokes equations.” *CALCOLO*, 21(4), 337–344.
- Aubry, R., Idelsohn, S., and Oñate, E. (2006). “Fractional step like schemes for free surface problems with thermal coupling using the lagrangian pfem.” *Computational Mechanics*, 38, 294–309.
- Bathe, K. and Wilson, E. (1972). “Large eigenvalue problems in synamic analysis.” *Journal of the Engineering Mechanics Division*, 98(6), 1471–1485.
- Becker, P., Idelsohn, S., and Oñate, E. (2015). “A unified monolithic approach for multi-fluid flows and fluid–structure interaction using the particle finite element method with fixed mesh.” *Computational Mechanics*, 55(6), 1091–1104.
- Calvo, N., Idelsohn, S. R., and Oñate, E. (2003). “The extended delaunay tessellation.” *Engineering Computations*, 20(5/6), 583–600.
- Chopra, A. K. (2007). *Dynamics of Structures: Theory and Applications to Earthquake Engineering*. Prentice-Hall, third edition.
- Cremonesi, M., Frangi, A., and Perego, U. (2010). “A Lagrangian finite element approach for the analysis of fluid-structure interaction problems.” *International Journal For Numerical Methods in Engineering*, 84, 610–630.
- Edelsbrunner, H. and Mücke, E. P. (1994). “Three-dimensional alpha shapes.” *ACM Transactions on Graphics*, 13(1), 43–72.
- Gresho, P. M. (1998). *Incompressible flow and the finite element method : advection-diffusion and isothermal laminar flow*. Chichester.
- Idelsohn, S., Marti, J., Limache, A., and Oñate, E. (2008). “Unified lagrangian formulation for elastic solids and incompressible fluids: Application to fluid-structure interaction problems via the pfem.” *Computer methods in applied mechanics and engineering*, 197, 1762–1776.
- Idelsohn, S., Pin, F. D., Rossi, R., and Oñate, E. (2009). “Fluid-structure interaction problems with strong added-mass effect.” *International Journal For Numerical Methods In Engineering*, 80, 1261–1294.
- Idelsohn, S. R. and Oñate, E. (2010). “The challenge of mass conservation in the solution of free-surface flows with the fractional-step method: Problems and solutions.” *International Journal for Numerical Methods in Biomedical Engineering*, 26, 1313–1330.
- Kaehler, R. C., White, D. W., and Kim, Y. D. (2011). *Frame Design Using Web-Tapered Members*. AISC.
- Mase, G. T., Smelser, R. E., and Mase, G. E. (2009). *Continuum Mechanics for Engineers*. CRC Press, third edition.
- McKenna, F., Scott, M. H., and Fenves, G. L. (2010). “Nonlinear finite-element analysis software architecture using object composition.” *Journal of Computing in Civil Engineering*, 24(1), 95–107.

- Oñate , E., Idelsohn, S., Del Pin, F., and Aubry, R. (2004). “ The Particle Finite Element Method. An Overview .” *International Journal of Computational Methods*, 1(2), 267–307.
- Oñate, E., Franci, A., and Carbonell, J. M. (2014). “Lagrangian formulation for finite element analysis of quasi-incompressible fluids with reduced mass losses.” *International Journal For Numerical Methods In Fluids*, 74(10), 699–731.
- Oñate, E., Idelsohn, S., Celigueta, M., Rossi, R., Martí, J., Carbonell, J., Ryzhakov, P., and Suárez, B. (2011). *Advances in the Particle Finite Element Method (PFEM) for Solving Coupled Problems in Engineering*. Springer Netherlands, Chapter 1, 1–49.
- Padgett, J., DesRoches, R., Nielson, B., Yashinsky, M., Kwon, O.-S., Burdette, N., and Tavera, E. (2008). “Bridge damage and repair costs from hurricane katrina.” *Journal of Bridge Engineering*, 13(1), 6–14.
- Rafiee, A. and Thiagarajan, K. P. (2009). “An sph projection method for simulating fluid-hypoelastic structure interaction.” *Computer Methods in Applied Mechanics and Engineering*, 198(33-36), 2785–2795.
- Ryzhakov, P., Rossi, R., Idelsohn, S., and Oñate, E. (2010). “ A monolithic Lagrangian approach for fluid-structure interaction problems .” *Comput. Mech.*, 46, 883–899.
- Simo, J. C. and Hughes, T. J. R. (1998). *Computational Inelasticity*. Springer-Verlag, New York, NY.
- Suppasri, A., Muhari, A., Ranasinghe, P., Mas, E., Imamura, F., and Koshimura, S. (2014). *Tsunami Events and Lessons Learned: Environmental and Societal Significance*. Springer Netherlands, Dordrecht, Chapter Damage and Reconstruction After the 2004 Indian Ocean Tsunami and the 2011 Tohoku Tsunami, 321–334.
- Walhorn, E., Kölke, A., Hübner, B., and Dinkler, D. (2005). “Fluid-structure coupling within a monolithic model involving free surface flows.” *Computers & Structures*, 83(25-26), 2100–2111.
- Watson, D. (1981). “Computing the n-dimensional delaunay tessellation with application to voronoi polytopes.” *The Computer Journal*, 24(2), 167–172.
- Welch, B. B. (2000). *Practical Programming in Tcl and Tk*. Perntice Hall, Upper Saddle River, NJ.
- Zhu, M. and Scott, M. H. (2014). “ Improved fractional step method for simulating fluid-structure interaction using the PFEM .” *International Journal for Numerical Methods in Engineering*, 99(12), 925–944.
- Zhu, M. and Scott, M. H. (2017). “ Unified fractional step method for Lagrangian analysis of quasi-incompressible fluid and nonlinear structure interaction using the PFEM .” *International Journal for Numerical Methods in Engineering*, 109(9), 1219–1236.
- Zienkiewicz, O., Taylor, R., and Zhu, J. (2005). *The Finite Element Method: Its Basis and Fundamentals*, Vol. 1. Elsevier Butterworth-Heinemann, sixth edition.

PEER REPORTS

PEER reports are available as a free PDF download from <https://peer.berkeley.edu/peer-reports>. In addition, printed hard copies of PEER reports can be ordered directly from our printer by following the instructions at <https://peer.berkeley.edu/peer-reports>. For other related questions about the PEER Report Series, contact the Pacific Earthquake Engineering Research Center, 325 Davis Hall, Mail Code 1792, Berkeley, CA 94720. Tel.: (510) 642-3437; and Email: peer_center@berkeley.edu.

- PEER 2019/05** *Expected Earthquake Performance of Buildings Designed to the California Building Code (California Alfred E. Alquist Seismic Safety Publication 19-01)*. Grace S. Kang, Sifat Muin, Jorge Archbold, Bitanoosh Woods, and Khalid Mosalam. July 2019.
- PEER 2019/04** *Aftershock Seismic Vulnerability and Time-Dependent Risk Assessment of Bridges*. Sujith Mangalathu, Mehrdad Shokrabiadi, and Henry V. Burton. May 2019.
- PEER 2019/03** *Ground-Motion Directivity Modeling for Seismic Hazard Applications*. Jennifer L. Donahue, Jonathan P. Stewart, Nicolas Gregor, and Yousef Bozorgnia. Review Panel: Jonathan D. Bray, Stephen A. Mahin, I. M. Idriss, Robert W. Graves, and Tom Shantz. May 2019.
- PEER 2019/02** *Direct-Finite-Element Method for Nonlinear Earthquake Analysis of Concrete Dams Including Dam–Water-Foundation Rock Interaction*. Arnkjell Løkke and Anil K. Chopra. March 2019.
- PEER 2019/01** *Flow-Failure Case History of the Las Palmas, Chile, Tailings Dam*. R. E. S. Moss, T. R. Gebhart, D. J. Frost, and C. Ledezma. January 2019.
- PEER 2018/08** *Central and Eastern North America Ground-Motion Characterization: NGA-East Final Report*. Christine Goulet, Yousef Bozorgnia, Norman Abrahamson, Nicolas Kuehn, Linda Al Atik, Robert Youngs, Robert Graves, and Gail Atkinson. December 2018.
- PEER 2018/07** *An Empirical Model for Fourier Amplitude Spectra using the NGA-West2 Database*. Jeff Bayless, and Norman A. Abrahamson. December 2018.
- PEER 2018/06** *Estimation of Shear Demands on Rock-Socketed Drilled Shafts subjected to Lateral Loading*. Pedro Arduino, Long Chen, and Christopher R. McGann. December 2018.
- PEER 2018/05** *Selection of Random Vibration Procedures for the NGA-East Project*. Albert Kottke, Norman A. Abrahamson, David M. Boore, Yousef Bozorgnia, Christine Goulet, Justin Hollenback, Tadahiro Kishida, Armen Der Kiureghian, Olga-Joan Ktenidou, Nicolas Kuehn, Ellen M. Rathje, Walter J. Silva, Eric Thompson, and Xiaoyue Wang. December 2018.
- PEER 2018/04** *Capturing Directivity Effects in the Mean and Aleatory Variability of the NGA-West 2 Ground Motion Prediction Equations*. Jennie A. Watson-Lamprey. November 2018.
- PEER 2018/03** *Probabilistic Seismic Hazard Analysis Code Verification*. Christie Hale, Norman Abrahamson, and Yousef Bozorgnia. July 2018.
- PEER 2018/02** *Update of the BCHydro Subduction Ground-Motion Model using the NGA-Subduction Dataset*. Norman Abrahamson, Nicolas Kuehn, Zeynep Gulerce, Nicholas Gregor, Yousef Bozorgnia, Grace Parker, Jonathan Stewart, Brian Chiou, I. M. Idriss, Kenneth Campbell, and Robert Youngs. June 2018.
- PEER 2018/01** *PEER Annual Report 2017–2018*. Khalid Mosalam, Amarnath Kasalanati, and Selim Günay. June 2018.
- PEER 2017/12** *Experimental Investigation of the Behavior of Vintage and Retrofit Concentrically Braced Steel Frames under Cyclic Loading*. Barbara G. Simpson, Stephen A. Mahin, and Jiun-Wei Lai, December 2017.
- PEER 2017/11** *Preliminary Studies on the Dynamic Response of a Seismically Isolated Prototype Gen-IV Sodium-Cooled Fast Reactor (PGSFR)*. Benshun Shao, Andreas H. Schellenberg, Matthew J. Schoettler, and Stephen A. Mahin. December 2017.
- PEER 2017/10** *Development of Time Histories for IEEE693 Testing and Analysis (including Seismically Isolated Equipment)*. Shakhzod M. Takhirov, Eric Fujisaki, Leon Kempner, Michael Riley, and Brian Low. December 2017.
- PEER 2017/09** *"R" Package for Computation of Earthquake Ground-Motion Response Spectra*. Pengfei Wang, Jonathan P. Stewart, Yousef Bozorgnia, David M. Boore, and Tadahiro Kishida. December 2017.
- PEER 2017/08** *Influence of Kinematic SSI on Foundation Input Motions for Bridges on Deep Foundations*. Benjamin J. Turner, Scott J. Brandenberg, and Jonathan P. Stewart. November 2017.
- PEER 2017/07** *A Nonlinear Kinetic Model for Multi-Stage Friction Pendulum Systems*. Paul L. Drazin and Sanjay Govindjee. September 2017.

- PEER 2017/06** *Guidelines for Performance-Based Seismic Design of Tall Buildings, Version 2.02.* TBI Working Group led by co-chairs Ron Hamburger and Jack Moehle; Jack Baker, Jonathan Bray, C.B. Crouse, Greg Deierlein, John Hooper, Marshall Lew, Joe Maffei, Stephen Mahin, James Malley, Farzad Naeim, Jonathan Stewart, and John Wallace. May 2017.
- PEER 2017/05** *Recommendations for Ergodic Nonlinear Site Amplification in Central and Eastern North America.* Youssef M.A. Hashash, Joseph A. Harmon, Okan Ilhan, Grace A. Parker, and Jonathan P. Stewart. March 2017.
- PEER 2017/04** *Expert Panel Recommendations for Ergodic Site Amplification in Central and Eastern North America.* Jonathan P. Stewart, Grace A. Parker, Joseph P. Harmon, Gail M. Atkinson, David M. Boore, Robert B. Darragh, Walter J. Silva, and Youssef M.A. Hashash. March 2017.
- PEER 2017/03** *NGA-East Ground-Motion Models for the U.S. Geological Survey National Seismic Hazard Maps.* Christine A. Goulet, Yousef Bozorgnia, Nicolas Kuehn, Linda Al Atik, Robert R. Youngs, Robert W. Graves, and Gail M. Atkinson. March 2017.
- PEER 2017/02** *U.S.–New Zealand–Japan Workshop: Liquefaction-Induced Ground Movements Effects, University of California, Berkeley, California, 2–4 November 2016.* Jonathan D. Bray, Ross W. Boulanger, Misko Cubrinovski, Kohji Tokimatsu, Steven L. Kramer, Thomas O'Rourke, Ellen Rathje, Russell A. Green, Peter K. Robinson, and Christine Z. Beyzaei. March 2017.
- PEER 2017/01** *2016 PEER Annual Report.* Khalid M. Mosalam, Amarnath Kasalanati, and Grace Kang. March 2017.
- PEER 2016/10** *Performance-Based Robust Nonlinear Seismic Analysis with Application to Reinforced Concrete Bridge Systems.* Xiao Ling and Khalid M. Mosalam. December 2016.
- PEER 2017/09** *Detailed Requirements for Column Plastic Hinges subjected to Combined Flexural, Axial, and Torsional Seismic Loading.* Gabriel Hurtado and Jack P. Moehle. December 2016.
- PEER 2016/08** *Resilience of Critical Structures, Infrastructure, and Communities.* Gian Paolo Cimellaro, Ali Zamani-Noori, Omar Kamouh, Vesna Terzic, and Stephen A. Mahin. December 2016.
- PEER 2016/07** *Hybrid Simulation Theory for a Classical Nonlinear Dynamical System.* Paul L. Drazin and Sanjay Govindjee. September 2016.
- PEER 2016/06** *California Earthquake Early Warning System Benefit Study.* Laurie A. Johnson, Sharyl Rabinovici, Grace S. Kang, and Stephen A. Mahin. July 2006.
- PEER 2016/05** *Ground-Motion Prediction Equations for Arias Intensity Consistent with the NGA-West2 Ground-Motion Models.* Charlotte Abrahamson, Hao-Jun Michael Shi, and Brian Yang. July 2016.
- PEER 2016/04** *The M_w 6.0 South Napa Earthquake of August 24, 2014: A Wake-Up Call for Renewed Investment in Seismic Resilience Across California.* Prepared for the California Seismic Safety Commission, Laurie A. Johnson and Stephen A. Mahin. May 2016.
- PEER 2016/03** *Simulation Confidence in Tsunami-Driven Overland Flow.* Patrick Lynett. May 2016.
- PEER 2016/02** *Semi-Automated Procedure for Windowing time Series and Computing Fourier Amplitude Spectra for the NGA-West2 Database.* Tadahiro Kishida, Olga-Joan Ktenidou, Robert B. Darragh, and Walter J. Silva. May 2016.
- PEER 2016/01** *A Methodology for the Estimation of Kappa (κ) from Large Datasets: Example Application to Rock Sites in the NGA-East Database and Implications on Design Motions.* Olga-Joan Ktenidou, Norman A. Abrahamson, Robert B. Darragh, and Walter J. Silva. April 2016.
- PEER 2015/13** *Self-Centering Precast Concrete Dual-Steel-Shell Columns for Accelerated Bridge Construction: Seismic Performance, Analysis, and Design.* Gabriele Guerrini, José I. Restrepo, Athanassios Vervelidis, and Milena Massari. December 2015.
- PEER 2015/12** *Shear-Flexure Interaction Modeling for Reinforced Concrete Structural Walls and Columns under Reversed Cyclic Loading.* Kristijan Kolozvari, Kutay Orakcal, and John Wallace. December 2015.
- PEER 2015/11** *Selection and Scaling of Ground Motions for Nonlinear Response History Analysis of Buildings in Performance-Based Earthquake Engineering.* N. Simon Kwong and Anil K. Chopra. December 2015.
- PEER 2015/10** *Structural Behavior of Column-Bent Cap Beam-Box Girder Systems in Reinforced Concrete Bridges Subjected to Gravity and Seismic Loads. Part II: Hybrid Simulation and Post-Test Analysis.* Mohamed A. Moustafa and Khalid M. Mosalam. November 2015.
- PEER 2015/09** *Structural Behavior of Column-Bent Cap Beam-Box Girder Systems in Reinforced Concrete Bridges Subjected to Gravity and Seismic Loads. Part I: Pre-Test Analysis and Quasi-Static Experiments.* Mohamed A. Moustafa and Khalid M. Mosalam. September 2015.
- PEER 2015/08** *NGA-East: Adjustments to Median Ground-Motion Models for Center and Eastern North America.* August 2015.

- PEER 2015/07** *NGA-East: Ground-Motion Standard-Deviation Models for Central and Eastern North America.* Linda Al Atik. June 2015.
- PEER 2015/06** *Adjusting Ground-Motion Intensity Measures to a Reference Site for which $V_{S30} = 3000$ m/sec.* David M. Boore. May 2015.
- PEER 2015/05** *Hybrid Simulation of Seismic Isolation Systems Applied to an APR-1400 Nuclear Power Plant.* Andreas H. Schellenberg, Alireza Sarebanha, Matthew J. Schoettler, Gilberto Mosqueda, Gianmario Benzoni, and Stephen A. Mahin. April 2015.
- PEER 2015/04** *NGA-East: Median Ground-Motion Models for the Central and Eastern North America Region.* April 2015.
- PEER 2015/03** *Single Series Solution for the Rectangular Fiber-Reinforced Elastomeric Isolator Compression Modulus.* James M. Kelly and Niel C. Van Engelen. March 2015.
- PEER 2015/02** *A Full-Scale, Single-Column Bridge Bent Tested by Shake-Table Excitation.* Matthew J. Schoettler, José I. Restrepo, Gabriele Guerrini, David E. Duck, and Francesco Carrea. March 2015.
- PEER 2015/01** *Concrete Column Blind Prediction Contest 2010: Outcomes and Observations.* Vesna Terzic, Matthew J. Schoettler, José I. Restrepo, and Stephen A Mahin. March 2015.
- PEER 2014/20** *Stochastic Modeling and Simulation of Near-Fault Ground Motions for Performance-Based Earthquake Engineering.* Mayssa Dabaghi and Armen Der Kiureghian. December 2014.
- PEER 2014/19** *Seismic Response of a Hybrid Fiber-Reinforced Concrete Bridge Column Detailed for Accelerated Bridge Construction.* Wilson Nguyen, William Trono, Marios Panagiotou, and Claudia P. Ostertag. December 2014.
- PEER 2014/18** *Three-Dimensional Beam-Truss Model for Reinforced Concrete Walls and Slabs Subjected to Cyclic Static or Dynamic Loading.* Yuan Lu, Marios Panagiotou, and Ioannis Koutromanos. December 2014.
- PEER 2014/17** *PEER NGA-East Database.* Christine A. Goulet, Tadahiro Kishida, Timothy D. Ancheta, Chris H. Cramer, Robert B. Darragh, Walter J. Silva, Youssef M.A. Hashash, Joseph Harmon, Jonathan P. Stewart, Katie E. Wooddell, and Robert R. Youngs. October 2014.
- PEER 2014/16** *Guidelines for Performing Hazard-Consistent One-Dimensional Ground Response Analysis for Ground Motion Prediction.* Jonathan P. Stewart, Kioumars Afshari, and Youssef M.A. Hashash. October 2014.
- PEER 2014/15** *NGA-East Regionalization Report: Comparison of Four Crustal Regions within Central and Eastern North America using Waveform Modeling and 5%-Damped Pseudo-Spectral Acceleration Response.* Jennifer Dreiling, Marius P. Isken, Walter D. Mooney, Martin C. Chapman, and Richard W. Godbee. October 2014.
- PEER 2014/14** *Scaling Relations between Seismic Moment and Rupture Area of Earthquakes in Stable Continental Regions.* Paul Somerville. August 2014.
- PEER 2014/13** *PEER Preliminary Notes and Observations on the August 24, 2014, South Napa Earthquake.* Grace S. Kang and Stephen A. Mahin, Editors. September 2014.
- PEER 2014/12** *Reference-Rock Site Conditions for Central and Eastern North America: Part II – Attenuation (Kappa) Definition.* Kenneth W. Campbell, Youssef M.A. Hashash, Byungmin Kim, Albert R. Kottke, Ellen M. Rathje, Walter J. Silva, and Jonathan P. Stewart. August 2014.
- PEER 2014/11** *Reference-Rock Site Conditions for Central and Eastern North America: Part I - Velocity Definition.* Youssef M.A. Hashash, Albert R. Kottke, Jonathan P. Stewart, Kenneth W. Campbell, Byungmin Kim, Ellen M. Rathje, Walter J. Silva, Sissy Nikolaou, and Cheryl Moss. August 2014.
- PEER 2014/10** *Evaluation of Collapse and Non-Collapse of Parallel Bridges Affected by Liquefaction and Lateral Spreading.* Benjamin Turner, Scott J. Brandenberg, and Jonathan P. Stewart. August 2014.
- PEER 2014/09** *PEER Arizona Strong-Motion Database and GMPEs Evaluation.* Tadahiro Kishida, Robert E. Kayen, Olga-Joan Ktenidou, Walter J. Silva, Robert B. Darragh, and Jennie Watson-Lamprey. June 2014.
- PEER 2014/08** *Unbonded Pretensioned Bridge Columns with Rocking Detail.* Jeffrey A. Schaefer, Bryan Kennedy, Marc O. Eberhard, and John F. Stanton. June 2014.
- PEER 2014/07** *Northridge 20 Symposium Summary Report: Impacts, Outcomes, and Next Steps.* May 2014.
- PEER 2014/06** *Report of the Tenth Planning Meeting of NEES/E-Defense Collaborative Research on Earthquake Engineering.* December 2013.
- PEER 2014/05** *Seismic Velocity Site Characterization of Thirty-One Chilean Seismometer Stations by Spectral Analysis of Surface Wave Dispersion.* Robert Kayen, Brad D. Carkin, Skye Corbet, Camilo Pinilla, Allan Ng, Edward Gorbis, and Christine Truong. April 2014.

- PEER 2014/04** Effect of Vertical Acceleration on Shear Strength of Reinforced Concrete Columns. Hyerin Lee and Khalid M. Mosalam. April 2014.
- PEER 2014/03** *Retest of Thirty-Year-Old Neoprene Isolation Bearings.* James M. Kelly and Niel C. Van Engelen. March 2014.
- PEER 2014/02** *Theoretical Development of Hybrid Simulation Applied to Plate Structures.* Ahmed A. Bakhaty, Khalid M. Mosalam, and Sanjay Govindjee. January 2014.
- PEER 2014/01** *Performance-Based Seismic Assessment of Skewed Bridges.* Peyman Kaviani, Farzin Zareian, and Ertugrul Taciroglu. January 2014.
- PEER 2013/26** *Urban Earthquake Engineering.* Proceedings of the U.S.-Iran Seismic Workshop. December 2013.
- PEER 2013/25** *Earthquake Engineering for Resilient Communities: 2013 PEER Internship Program Research Report Collection.* Heidi Tremayne (Editor), Stephen A. Mahin (Editor), Jorge Archbold Monterossa, Matt Brosman, Shelly Dean, Katherine deLaveaga, Curtis Fong, Donovan Holder, Rakeeb Khan, Elizabeth Jachens, David Lam, Daniela Martinez Lopez, Mara Minner, Geffen Oren, Julia Pavicic, Melissa Quinonez, Lorena Rodriguez, Sean Salazar, Kelli Slaven, Vivian Steyert, Jenny Taing, and Salvador Tena. December 2013.
- PEER 2013/24** *NGA-West2 Ground Motion Prediction Equations for Vertical Ground Motions.* September 2013.
- PEER 2013/23** *Coordinated Planning and Preparedness for Fire Following Major Earthquakes.* Charles Scawthorn. November 2013.
- PEER 2013/22** *GEM-PEER Task 3 Project: Selection of a Global Set of Ground Motion Prediction Equations.* Jonathan P. Stewart, John Douglas, Mohammad B. Javanbarg, Carola Di Alessandro, Yousef Bozorgnia, Norman A. Abrahamson, David M. Boore, Kenneth W. Campbell, Elise Delavaud, Mustafa Erdik, and Peter J. Stafford. December 2013.
- PEER 2013/21** *Seismic Design and Performance of Bridges with Columns on Rocking Foundations.* Grigorios Antonellis and Marios Panagiotou. September 2013.
- PEER 2013/20** *Experimental and Analytical Studies on the Seismic Behavior of Conventional and Hybrid Braced Frames.* Jiun-Wei Lai and Stephen A. Mahin. September 2013.
- PEER 2013/19** *Toward Resilient Communities: A Performance-Based Engineering Framework for Design and Evaluation of the Built Environment.* Michael William Mieler, Bozidar Stojadinovic, Robert J. Budnitz, Stephen A. Mahin, and Mary C. Comerio. September 2013.
- PEER 2013/18** *Identification of Site Parameters that Improve Predictions of Site Amplification.* Ellen M. Rathje and Sara Navidi. July 2013.
- PEER 2013/17** *Response Spectrum Analysis of Concrete Gravity Dams Including Dam-Water-Foundation Interaction.* Arnkjell Løkke and Anil K. Chopra. July 2013.
- PEER 2013/16** *Effect of Hoop Reinforcement Spacing on the Cyclic Response of Large Reinforced Concrete Special Moment Frame Beams.* Marios Panagiotou, Tea Visnjic, Grigorios Antonellis, Panagiotis Galanis, and Jack P. Moehle. June 2013.
- PEER 2013/15** *A Probabilistic Framework to Include the Effects of Near-Fault Directivity in Seismic Hazard Assessment.* Shrey Kumar Shahi, Jack W. Baker. October 2013.
- PEER 2013/14** *Hanging-Wall Scaling using Finite-Fault Simulations.* Jennifer L. Donahue and Norman A. Abrahamson. September 2013.
- PEER 2013/13** *Semi-Empirical Nonlinear Site Amplification and its Application in NEHRP Site Factors.* Jonathan P. Stewart and Emel Seyhan. November 2013.
- PEER 2013/12** *Nonlinear Horizontal Site Response for the NGA-West2 Project.* Ronnie Kamai, Norman A. Abramson, Walter J. Silva. May 2013.
- PEER 2013/11** *Epistemic Uncertainty for NGA-West2 Models.* Linda Al Atik and Robert R. Youngs. May 2013.
- PEER 2013/10** *NGA-West 2 Models for Ground-Motion Directionality.* Shrey K. Shahi and Jack W. Baker. May 2013.
- PEER 2013/09** *Final Report of the NGA-West2 Directivity Working Group.* Paul Spudich, Jeffrey R. Bayless, Jack W. Baker, Brian S.J. Chiou, Badie Rowshandel, Shrey Shahi, and Paul Somerville. May 2013.
- PEER 2013/08** *NGA-West2 Model for Estimating Average Horizontal Values of Pseudo-Absolute Spectral Accelerations Generated by Crustal Earthquakes.* I. M. Idriss. May 2013.
- PEER 2013/07** *Update of the Chiou and Youngs NGA Ground Motion Model for Average Horizontal Component of Peak Ground Motion and Response Spectra.* Brian Chiou and Robert Youngs. May 2013.

- PEER 2013/06** *NGA-West2 Campbell-Bozorgnia Ground Motion Model for the Horizontal Components of PGA, PGV, and 5%-Damped Elastic Pseudo-Acceleration Response Spectra for Periods Ranging from 0.01 to 10 sec.* Kenneth W. Campbell and Yousef Bozorgnia. May 2013.
- PEER 2013/05** *NGA-West 2 Equations for Predicting Response Spectral Accelerations for Shallow Crustal Earthquakes.* David M. Boore, Jonathan P. Stewart, Emel Seyhan, and Gail M. Atkinson. May 2013.
- PEER 2013/04** *Update of the AS08 Ground-Motion Prediction Equations Based on the NGA-West2 Data Set.* Norman Abrahamson, Walter Silva, and Ronnie Kamai. May 2013.
- PEER 2013/03** *PEER NGA-West2 Database.* Timothy D. Ancheta, Robert B. Darragh, Jonathan P. Stewart, Emel Seyhan, Walter J. Silva, Brian S.J. Chiou, Katie E. Wooddell, Robert W. Graves, Albert R. Kottke, David M. Boore, Tadahiro Kishida, and Jennifer L. Donahue. May 2013.
- PEER 2013/02** *Hybrid Simulation of the Seismic Response of Squat Reinforced Concrete Shear Walls.* Catherine A. Whyte and Bozidar Stojadinovic. May 2013.
- PEER 2013/01** *Housing Recovery in Chile: A Qualitative Mid-program Review.* Mary C. Comerio. February 2013.
- PEER 2012/08** *Guidelines for Estimation of Shear Wave Velocity.* Bernard R. Wair, Jason T. DeJong, and Thomas Shantz. December 2012.
- PEER 2012/07** *Earthquake Engineering for Resilient Communities: 2012 PEER Internship Program Research Report Collection.* Heidi Tremayne (Editor), Stephen A. Mahin (Editor), Collin Anderson, Dustin Cook, Michael Erceg, Carlos Esparza, Jose Jimenez, Dorian Krausz, Andrew Lo, Stephanie Lopez, Nicole McCurdy, Paul Shipman, Alexander Strum, Eduardo Vega. December 2012.
- PEER 2012/06** *Fragilities for Precarious Rocks at Yucca Mountain.* Matthew D. Purvance, Rasool Anooshehpoor, and James N. Brune. December 2012.
- PEER 2012/05** *Development of Simplified Analysis Procedure for Piles in Laterally Spreading Layered Soils.* Christopher R. McGann, Pedro Arduino, and Peter Mackenzie-Helnwein. December 2012.
- PEER 2012/04** *Unbonded Pre-Tensioned Columns for Bridges in Seismic Regions.* Phillip M. Davis, Todd M. Janes, Marc O. Eberhard, and John F. Stanton. December 2012.
- PEER 2012/03** *Experimental and Analytical Studies on Reinforced Concrete Buildings with Seismically Vulnerable Beam-Column Joints.* Sangjoon Park and Khalid M. Mosalam. October 2012.
- PEER 2012/02** *Seismic Performance of Reinforced Concrete Bridges Allowed to Uplift during Multi-Directional Excitation.* Andres Oscar Espinoza and Stephen A. Mahin. July 2012.
- PEER 2012/01** *Spectral Damping Scaling Factors for Shallow Crustal Earthquakes in Active Tectonic Regions.* Sanaz Rezaeian, Yousef Bozorgnia, I. M. Idriss, Kenneth Campbell, Norman Abrahamson, and Walter Silva. July 2012.
- PEER 2011/10** *Earthquake Engineering for Resilient Communities: 2011 PEER Internship Program Research Report Collection.* Heidi Faison and Stephen A. Mahin, Editors. December 2011.
- PEER 2011/09** *Calibration of Semi-Stochastic Procedure for Simulating High-Frequency Ground Motions.* Jonathan P. Stewart, Emel Seyhan, and Robert W. Graves. December 2011.
- PEER 2011/08** *Water Supply in regard to Fire Following Earthquake.* Charles Scawthorn. November 2011.
- PEER 2011/07** *Seismic Risk Management in Urban Areas.* Proceedings of a U.S.-Iran-Turkey Seismic Workshop. September 2011.
- PEER 2011/06** *The Use of Base Isolation Systems to Achieve Complex Seismic Performance Objectives.* Troy A. Morgan and Stephen A. Mahin. July 2011.
- PEER 2011/05** *Case Studies of the Seismic Performance of Tall Buildings Designed by Alternative Means.* Task 12 Report for the Tall Buildings Initiative. Jack Moehle, Yousef Bozorgnia, Nirmal Jayaram, Pierson Jones, Mohsen Rahnama, Nilesh Shome, Zeynep Tuna, John Wallace, Tony Yang, and Farzin Zareian. July 2011.
- PEER 2011/04** *Recommended Design Practice for Pile Foundations in Laterally Spreading Ground.* Scott A. Ashford, Ross W. Boulanger, and Scott J. Brandenberg. June 2011.
- PEER 2011/03** *New Ground Motion Selection Procedures and Selected Motions for the PEER Transportation Research Program.* Jack W. Baker, Ting Lin, Shrey K. Shahi, and Nirmal Jayaram. March 2011.
- PEER 2011/02** *A Bayesian Network Methodology for Infrastructure Seismic Risk Assessment and Decision Support.* Michelle T. Bensi, Armen Der Kiureghian, and Daniel Straub. March 2011.
- PEER 2011/01** *Demand Fragility Surfaces for Bridges in Liquefied and Laterally Spreading Ground.* Scott J. Brandenberg, Jian Zhang, Pirooz Kashighandi, Yili Huo, and Minxing Zhao. March 2011.

- PEER 2010/05** *Guidelines for Performance-Based Seismic Design of Tall Buildings.* Developed by the Tall Buildings Initiative. November 2010.
- PEER 2010/04** *Application Guide for the Design of Flexible and Rigid Bus Connections between Substation Equipment Subjected to Earthquakes.* Jean-Bernard Dastous and Armen Der Kiureghian. September 2010.
- PEER 2010/03** *Shear Wave Velocity as a Statistical Function of Standard Penetration Test Resistance and Vertical Effective Stress at Caltrans Bridge Sites.* Scott J. Brandenberg, Naresh Bellana, and Thomas Shantz. June 2010.
- PEER 2010/02** *Stochastic Modeling and Simulation of Ground Motions for Performance-Based Earthquake Engineering.* Sanaz Rezaeian and Armen Der Kiureghian. June 2010.
- PEER 2010/01** *Structural Response and Cost Characterization of Bridge Construction Using Seismic Performance Enhancement Strategies.* Ady Aviram, Božidar Stojadinović, Gustavo J. Parra-Montesinos, and Kevin R. Mackie. March 2010.
- PEER 2009/03** *The Integration of Experimental and Simulation Data in the Study of Reinforced Concrete Bridge Systems Including Soil-Foundation-Structure Interaction.* Matthew Dryden and Gregory L. Fenves. November 2009.
- PEER 2009/02** *Improving Earthquake Mitigation through Innovations and Applications in Seismic Science, Engineering, Communication, and Response.* Proceedings of a U.S.-Iran Seismic Workshop. October 2009.
- PEER 2009/01** *Evaluation of Ground Motion Selection and Modification Methods: Predicting Median Interstory Drift Response of Buildings.* Curt B. Haselton, Editor. June 2009.
- PEER 2008/10** *Technical Manual for Strata.* Albert R. Kottke and Ellen M. Rathje. February 2009.
- PEER 2008/09** *NGA Model for Average Horizontal Component of Peak Ground Motion and Response Spectra.* Brian S.-J. Chiou and Robert R. Youngs. November 2008.
- PEER 2008/08** *Toward Earthquake-Resistant Design of Concentrically Braced Steel Structures.* Patxi Uriz and Stephen A. Mahin. November 2008.
- PEER 2008/07** *Using OpenSees for Performance-Based Evaluation of Bridges on Liquefiable Soils.* Stephen L. Kramer, Pedro Arduino, and HyungSuk Shin. November 2008.
- PEER 2008/06** *Shaking Table Tests and Numerical Investigation of Self-Centering Reinforced Concrete Bridge Columns.* Hyung IL Jeong, Junichi Sakai, and Stephen A. Mahin. September 2008.
- PEER 2008/05** *Performance-Based Earthquake Engineering Design Evaluation Procedure for Bridge Foundations Undergoing Liquefaction-Induced Lateral Ground Displacement.* Christian A. Ledezma and Jonathan D. Bray. August 2008.
- PEER 2008/04** *Benchmarking of Nonlinear Geotechnical Ground Response Analysis Procedures.* Jonathan P. Stewart, Annie On-Lei Kwok, Youssef M. A. Hashash, Neven Matasovic, Robert Pyke, Zhiliang Wang, and Zhao Hui Yang. August 2008.
- PEER 2008/03** *Guidelines for Nonlinear Analysis of Bridge Structures in California.* Ady Aviram, Kevin R. Mackie, and Božidar Stojadinović. August 2008.
- PEER 2008/02** *Treatment of Uncertainties in Seismic-Risk Analysis of Transportation Systems.* Evangelos Stergiou and Anne S. Kiremidjian. July 2008.
- PEER 2008/01** *Seismic Performance Objectives for Tall Buildings.* William T. Holmes, Charles Kircher, William Petak, and Nabih Youssef. August 2008.
- PEER 2007/12** *An Assessment to Benchmark the Seismic Performance of a Code-Conforming Reinforced Concrete Moment-Frame Building.* Curt Haselton, Christine A. Goulet, Judith Mitrani-Reiser, James L. Beck, Gregory G. Deierlein, Keith A. Porter, Jonathan P. Stewart, and Ertugrul Taciroglu. August 2008.
- PEER 2007/11** *Bar Buckling in Reinforced Concrete Bridge Columns.* Wayne A. Brown, Dawn E. Lehman, and John F. Stanton. February 2008.
- PEER 2007/10** *Computational Modeling of Progressive Collapse in Reinforced Concrete Frame Structures.* Mohamed M. Talaat and Khalid M. Mosalam. May 2008.
- PEER 2007/09** *Integrated Probabilistic Performance-Based Evaluation of Benchmark Reinforced Concrete Bridges.* Kevin R. Mackie, John-Michael Wong, and Božidar Stojadinović. January 2008.
- PEER 2007/08** *Assessing Seismic Collapse Safety of Modern Reinforced Concrete Moment-Frame Buildings.* Curt B. Haselton and Gregory G. Deierlein. February 2008.
- PEER 2007/07** *Performance Modeling Strategies for Modern Reinforced Concrete Bridge Columns.* Michael P. Berry and Marc O. Eberhard. April 2008.

- PEER 2007/06** *Development of Improved Procedures for Seismic Design of Buried and Partially Buried Structures.* Linda Al Atik and Nicholas Sitar. June 2007.
- PEER 2007/05** *Uncertainty and Correlation in Seismic Risk Assessment of Transportation Systems.* Renee G. Lee and Anne S. Kiremidjian. July 2007.
- PEER 2007/04** *Numerical Models for Analysis and Performance-Based Design of Shallow Foundations Subjected to Seismic Loading.* Sivapalan Gajan, Tara C. Hutchinson, Bruce L. Kutter, Prishati Raychowdhury, José A. Ugalde, and Jonathan P. Stewart. May 2008.
- PEER 2007/03** *Beam-Column Element Model Calibrated for Predicting Flexural Response Leading to Global Collapse of RC Frame Buildings.* Curt B. Haselton, Abbie B. Liel, Sarah Taylor Lange, and Gregory G. Deierlein. May 2008.
- PEER 2007/02** *Campbell-Bozorgnia NGA Ground Motion Relations for the Geometric Mean Horizontal Component of Peak and Spectral Ground Motion Parameters.* Kenneth W. Campbell and Yousef Bozorgnia. May 2007.
- PEER 2007/01** *Boore-Atkinson NGA Ground Motion Relations for the Geometric Mean Horizontal Component of Peak and Spectral Ground Motion Parameters.* David M. Boore and Gail M. Atkinson. May 2007.
- PEER 2006/12** Societal Implications of Performance-Based Earthquake Engineering. Peter J. May. May 2007.
- PEER 2006/11** *Probabilistic Seismic Demand Analysis Using Advanced Ground Motion Intensity Measures, Attenuation Relationships, and Near-Fault Effects.* Polsak Tothong and C. Allin Cornell. March 2007.
- PEER 2006/10** *Application of the PEER PBEE Methodology to the I-880 Viaduct.* Sashi Kunnath. February 2007.
- PEER 2006/09** *Quantifying Economic Losses from Travel Forgone Following a Large Metropolitan Earthquake.* James Moore, Sungbin Cho, Yue Yue Fan, and Stuart Werner. November 2006.
- PEER 2006/08** *Vector-Valued Ground Motion Intensity Measures for Probabilistic Seismic Demand Analysis.* Jack W. Baker and C. Allin Cornell. October 2006.
- PEER 2006/07** *Analytical Modeling of Reinforced Concrete Walls for Predicting Flexural and Coupled-Shear-Flexural Responses.* Kutay Orakcal, Leonardo M. Massone, and John W. Wallace. October 2006.
- PEER 2006/06** *Nonlinear Analysis of a Soil-Drilled Pier System under Static and Dynamic Axial Loading.* Gang Wang and Nicholas Sitar. November 2006.
- PEER 2006/05** *Advanced Seismic Assessment Guidelines.* Paolo Bazzurro, C. Allin Cornell, Charles Menun, Maziar Motahari, and Nicolas Luco. September 2006.
- PEER 2006/04** *Probabilistic Seismic Evaluation of Reinforced Concrete Structural Components and Systems.* Tae Hyung Lee and Khalid M. Mosalam. August 2006.
- PEER 2006/03** *Performance of Lifelines Subjected to Lateral Spreading.* Scott A. Ashford and Teerawut Juimarrongrit. July 2006.
- PEER 2006/02** *Pacific Earthquake Engineering Research Center Highway Demonstration Project.* Anne Kiremidjian, James Moore, Yue Yue Fan, Nesrin Basoz, Ozgur Yazali, and Meredith Williams. April 2006.
- PEER 2006/01** *Bracing Berkeley. A Guide to Seismic Safety on the UC Berkeley Campus.* Mary C. Comerio, Stephen Tobriner, and Ariane Fehrenkamp. January 2006.
- PEER 2005/17** *Earthquake Simulation Tests on Reducing Residual Displacements of Reinforced Concrete Bridges.* Junichi Sakai, Stephen A Mahin, and Andres Espinoza. December 2005.
- PEER 2005/16** *Seismic Response and Reliability of Electrical Substation Equipment and Systems.* Junho Song, Armen Der Kiureghian, and Jerome L. Sackman. April 2006.
- PEER 2005/15** *CPT-Based Probabilistic Assessment of Seismic Soil Liquefaction Initiation.* R. E. S. Moss, R. B. Seed, R. E. Kayen, J. P. Stewart, and A. Der Kiureghian. April 2006.
- PEER 2005/14** *Workshop on Modeling of Nonlinear Cyclic Load-Deformation Behavior of Shallow Foundations.* Bruce L. Kutter, Geoffrey Martin, Tara Hutchinson, Chad Harden, Sivapalan Gajan, and Justin Phalen. March 2006.
- PEER 2005/13** *Stochastic Characterization and Decision Bases under Time-Dependent Aftershock Risk in Performance-Based Earthquake Engineering.* Gee Liek Yeo and C. Allin Cornell. July 2005.
- PEER 2005/12** *PEER Testbed Study on a Laboratory Building: Exercising Seismic Performance Assessment.* Mary C. Comerio, Editor. November 2005.
- PEER 2005/11** *Van Nuys Hotel Building Testbed Report: Exercising Seismic Performance Assessment.* Helmut Krawinkler, Editor. October 2005.

- PEER 2005/10** *First NEES/E-Defense Workshop on Collapse Simulation of Reinforced Concrete Building Structures.* September 2005.
- PEER 2005/09** *Test Applications of Advanced Seismic Assessment Guidelines.* Joe Maffei, Karl Telleen, Danya Mohr, William Holmes, and Yuki Nakayama. August 2006.
- PEER 2005/08** *Damage Accumulation in Lightly Confined Reinforced Concrete Bridge Columns.* R. Tyler Ranf, Jared M. Nelson, Zach Price, Marc O. Eberhard, and John F. Stanton. April 2006.
- PEER 2005/07** *Experimental and Analytical Studies on the Seismic Response of Freestanding and Anchored Laboratory Equipment.* Dimitrios Konstantinidis and Nicos Makris. January 2005.
- PEER 2005/06** *Global Collapse of Frame Structures under Seismic Excitations.* Luis F. Ibarra and Helmut Krawinkler. September 2005.
- PEER 2005/05** *Performance Characterization of Bench- and Shelf-Mounted Equipment.* Samit Ray Chaudhuri and Tara C. Hutchinson. May 2006.
- PEER 2005/04** *Numerical Modeling of the Nonlinear Cyclic Response of Shallow Foundations.* Chad Harden, Tara Hutchinson, Geoffrey R. Martin, and Bruce L. Kutter. August 2005.
- PEER 2005/03** *A Taxonomy of Building Components for Performance-Based Earthquake Engineering.* Keith A. Porter. September 2005.
- PEER 2005/02** *Fragility Basis for California Highway Overpass Bridge Seismic Decision Making.* Kevin R. Mackie and Božidar Stojadinović. June 2005.
- PEER 2005/01** *Empirical Characterization of Site Conditions on Strong Ground Motion.* Jonathan P. Stewart, Yoojoong Choi, and Robert W. Graves. June 2005.
- PEER 2004/09** *Electrical Substation Equipment Interaction: Experimental Rigid Conductor Studies.* Christopher Stearns and André Filiault. February 2005.
- PEER 2004/08** *Seismic Qualification and Fragility Testing of Line Break 550-kV Disconnect Switches.* Shakhzod M. Takhirov, Gregory L. Fenves, and Eric Fujisaki. January 2005.
- PEER 2004/07** *Ground Motions for Earthquake Simulator Qualification of Electrical Substation Equipment.* Shakhzod M. Takhirov, Gregory L. Fenves, Eric Fujisaki, and Don Clyde. January 2005.
- PEER 2004/06** *Performance-Based Regulation and Regulatory Regimes.* Peter J. May and Chris Koski. September 2004.
- PEER 2004/05** *Performance-Based Seismic Design Concepts and Implementation: Proceedings of an International Workshop.* Peter Fajfar and Helmut Krawinkler, Editors. September 2004.
- PEER 2004/04** *Seismic Performance of an Instrumented Tilt-up Wall Building.* James C. Anderson and Vitelmo V. Bertero. July 2004.
- PEER 2004/03** *Evaluation and Application of Concrete Tilt-up Assessment Methodologies.* Timothy Graf and James O. Malley. October 2004.
- PEER 2004/02** *Analytical Investigations of New Methods for Reducing Residual Displacements of Reinforced Concrete Bridge Columns.* Junichi Sakai and Stephen A. Mahin. August 2004.
- PEER 2004/01** *Seismic Performance of Masonry Buildings and Design Implications.* Kerri Anne Taeko Tokoro, James C. Anderson, and Vitelmo V. Bertero. February 2004.
- PEER 2003/18** *Performance Models for Flexural Damage in Reinforced Concrete Columns.* Michael Berry and Marc Eberhard. August 2003.
- PEER 2003/17** *Predicting Earthquake Damage in Older Reinforced Concrete Beam-Column Joints.* Catherine Pagni and Laura Lowes. October 2004.
- PEER 2003/16** *Seismic Demands for Performance-Based Design of Bridges.* Kevin Mackie and Božidar Stojadinović. August 2003.
- PEER 2003/15** *Seismic Demands for Nondeteriorating Frame Structures and Their Dependence on Ground Motions.* Ricardo Antonio Medina and Helmut Krawinkler. May 2004.
- PEER 2003/14** *Finite Element Reliability and Sensitivity Methods for Performance-Based Earthquake Engineering.* Terje Haukaas and Armen Der Kiureghian. April 2004.
- PEER 2003/13** *Effects of Connection Hysteretic Degradation on the Seismic Behavior of Steel Moment-Resisting Frames.* Janise E. Rodgers and Stephen A. Mahin. March 2004.

- PEER 2003/12** *Implementation Manual for the Seismic Protection of Laboratory Contents: Format and Case Studies.* William T. Holmes and Mary C. Comerio. October 2003.
- PEER 2003/11** *Fifth U.S.-Japan Workshop on Performance-Based Earthquake Engineering Methodology for Reinforced Concrete Building Structures.* February 2004.
- PEER 2003/10** *A Beam-Column Joint Model for Simulating the Earthquake Response of Reinforced Concrete Frames.* Laura N. Lowes, Nilanjan Mitra, and Arash Altoontash. February 2004.
- PEER 2003/09** *Sequencing Repairs after an Earthquake: An Economic Approach.* Marco Casari and Simon J. Wilkie. April 2004.
- PEER 2003/08** *A Technical Framework for Probability-Based Demand and Capacity Factor Design (DCFD) Seismic Formats.* Fatemeh Jalayer and C. Allin Cornell. November 2003.
- PEER 2003/07** *Uncertainty Specification and Propagation for Loss Estimation Using FOSM Methods.* Jack W. Baker and C. Allin Cornell. September 2003.
- PEER 2003/06** *Performance of Circular Reinforced Concrete Bridge Columns under Bidirectional Earthquake Loading.* Mahmoud M. Hachem, Stephen A. Mahin, and Jack P. Moehle. February 2003.
- PEER 2003/05** *Response Assessment for Building-Specific Loss Estimation.* Eduardo Miranda and Shahram Taghavi. September 2003.
- PEER 2003/04** *Experimental Assessment of Columns with Short Lap Splices Subjected to Cyclic Loads.* Murat Melek, John W. Wallace, and Joel Conte. April 2003.
- PEER 2003/03** *Probabilistic Response Assessment for Building-Specific Loss Estimation.* Eduardo Miranda and Hesameddin Aslani. September 2003.
- PEER 2003/02** *Software Framework for Collaborative Development of Nonlinear Dynamic Analysis Program.* Jun Peng and Kincho H. Law. September 2003.
- PEER 2003/01** *Shake Table Tests and Analytical Studies on the Gravity Load Collapse of Reinforced Concrete Frames.* Kenneth John Elwood and Jack P. Moehle. November 2003.
- PEER 2002/24** *Performance of Beam to Column Bridge Joints Subjected to a Large Velocity Pulse.* Natalie Gibson, André Filiault, and Scott A. Ashford. April 2002.
- PEER 2002/23** *Effects of Large Velocity Pulses on Reinforced Concrete Bridge Columns.* Greg L. Orozco and Scott A. Ashford. April 2002.
- PEER 2002/22** *Characterization of Large Velocity Pulses for Laboratory Testing.* Kenneth E. Cox and Scott A. Ashford. April 2002.
- PEER 2002/21** *Fourth U.S.-Japan Workshop on Performance-Based Earthquake Engineering Methodology for Reinforced Concrete Building Structures.* December 2002.
- PEER 2002/20** *Barriers to Adoption and Implementation of PBEE Innovations.* Peter J. May. August 2002.
- PEER 2002/19** *Economic-Engineered Integrated Models for Earthquakes: Socioeconomic Impacts.* Peter Gordon, James E. Moore II, and Harry W. Richardson. July 2002.
- PEER 2002/18** *Assessment of Reinforced Concrete Building Exterior Joints with Substandard Details.* Chris P. Pantelides, Jon Hansen, Justin Nadauld, and Lawrence D. Reaveley. May 2002.
- PEER 2002/17** *Structural Characterization and Seismic Response Analysis of a Highway Overcrossing Equipped with Elastomeric Bearings and Fluid Dampers: A Case Study.* Nicos Makris and Jian Zhang. November 2002.
- PEER 2002/16** *Estimation of Uncertainty in Geotechnical Properties for Performance-Based Earthquake Engineering.* Allen L. Jones, Steven L. Kramer, and Pedro Arduino. December 2002.
- PEER 2002/15** *Seismic Behavior of Bridge Columns Subjected to Various Loading Patterns.* Asadollah Esmaeily-Gh. and Yan Xiao. December 2002.
- PEER 2002/14** *Inelastic Seismic Response of Extended Pile Shaft Supported Bridge Structures.* T.C. Hutchinson, R.W. Boulanger, Y.H. Chai, and I.M. Idriss. December 2002.
- PEER 2002/13** *Probabilistic Models and Fragility Estimates for Bridge Components and Systems.* Paolo Gardoni, Armen Der Kiureghian, and Khalid M. Mosalam. June 2002.
- PEER 2002/12** *Effects of Fault Dip and Slip Rake on Near-Source Ground Motions: Why Chi-Chi Was a Relatively Mild M7.6 Earthquake.* Brad T. Aagaard, John F. Hall, and Thomas H. Heaton. December 2002.

- PEER 2002/11** *Analytical and Experimental Study of Fiber-Reinforced Strip Isolators.* James M. Kelly and Shakhzod M. Takhirov. September 2002.
- PEER 2002/10** *Centrifuge Modeling of Settlement and Lateral Spreading with Comparisons to Numerical Analyses.* Sivapalan Gajan and Bruce L. Kutter. January 2003.
- PEER 2002/09** *Documentation and Analysis of Field Case Histories of Seismic Compression during the 1994 Northridge, California, Earthquake.* Jonathan P. Stewart, Patrick M. Smith, Daniel H. Whang, and Jonathan D. Bray. October 2002.
- PEER 2002/08** *Component Testing, Stability Analysis and Characterization of Buckling-Restrained Unbonded BracesTM.* Cameron Black, Nicos Makris, and Ian Aiken. September 2002.
- PEER 2002/07** *Seismic Performance of Pile-Wharf Connections.* Charles W. Roeder, Robert Graff, Jennifer Soderstrom, and Jun Han Yoo. December 2001.
- PEER 2002/06** *The Use of Benefit-Cost Analysis for Evaluation of Performance-Based Earthquake Engineering Decisions.* Richard O. Zerbe and Anthony Falit-Baiamonte. September 2001.
- PEER 2002/05** *Guidelines, Specifications, and Seismic Performance Characterization of Nonstructural Building Components and Equipment.* André Filiault, Constantin Christopoulos, and Christopher Stearns. September 2001.
- PEER 2002/04** *Consortium of Organizations for Strong-Motion Observation Systems and the Pacific Earthquake Engineering Research Center Lifelines Program: Invited Workshop on Archiving and Web Dissemination of Geotechnical Data, 4–5 October 2001.* September 2002.
- PEER 2002/03** *Investigation of Sensitivity of Building Loss Estimates to Major Uncertain Variables for the Van Nuys Testbed.* Keith A. Porter, James L. Beck, and Rustem V. Shaikhutdinov. August 2002.
- PEER 2002/02** *The Third U.S.-Japan Workshop on Performance-Based Earthquake Engineering Methodology for Reinforced Concrete Building Structures.* July 2002.
- PEER 2002/01** *Nonstructural Loss Estimation: The UC Berkeley Case Study.* Mary C. Comerio and John C. Stallmeyer. December 2001.
- PEER 2001/16** *Statistics of SDF-System Estimate of Roof Displacement for Pushover Analysis of Buildings.* Anil K. Chopra, Rakesh K. Goel, and Chatpan Chintanapakdee. December 2001.
- PEER 2001/15** *Damage to Bridges during the 2001 Nisqually Earthquake.* R. Tyler Ranf, Marc O. Eberhard, and Michael P. Berry. November 2001.
- PEER 2001/14** *Rocking Response of Equipment Anchored to a Base Foundation.* Nicos Makris and Cameron J. Black. September 2001.
- PEER 2001/13** *Modeling Soil Liquefaction Hazards for Performance-Based Earthquake Engineering.* Steven L. Kramer and Ahmed-W. Elgamal. February 2001.
- PEER 2001/12** *Development of Geotechnical Capabilities in OpenSees.* Boris Jeremić. September 2001.
- PEER 2001/11** *Analytical and Experimental Study of Fiber-Reinforced Elastomeric Isolators.* James M. Kelly and Shakhzod M. Takhirov. September 2001.
- PEER 2001/10** *Amplification Factors for Spectral Acceleration in Active Regions.* Jonathan P. Stewart, Andrew H. Liu, Yoojoong Choi, and Mehmet B. Baturay. December 2001.
- PEER 2001/09** *Ground Motion Evaluation Procedures for Performance-Based Design.* Jonathan P. Stewart, Shyh-Jeng Chiou, Jonathan D. Bray, Robert W. Graves, Paul G. Somerville, and Norman A. Abrahamson. September 2001.
- PEER 2001/08** *Experimental and Computational Evaluation of Reinforced Concrete Bridge Beam-Column Connections for Seismic Performance.* Clay J. Naito, Jack P. Moehle, and Khalid M. Mosalam. November 2001.
- PEER 2001/07** *The Rocking Spectrum and the Shortcomings of Design Guidelines.* Nicos Makris and Dimitrios Konstantinidis. August 2001.
- PEER 2001/06** *Development of an Electrical Substation Equipment Performance Database for Evaluation of Equipment Fragilities.* Thalia Agnanos. April 1999.
- PEER 2001/05** *Stiffness Analysis of Fiber-Reinforced Elastomeric Isolators.* Hsiang-Chuan Tsai and James M. Kelly. May 2001.
- PEER 2001/04** *Organizational and Societal Considerations for Performance-Based Earthquake Engineering.* Peter J. May. April 2001.
- PEER 2001/03** *A Modal Pushover Analysis Procedure to Estimate Seismic Demands for Buildings: Theory and Preliminary Evaluation.* Anil K. Chopra and Rakesh K. Goel. January 2001.

- PEER 2001/02** *Seismic Response Analysis of Highway Overcrossings Including Soil-Structure Interaction.* Jian Zhang and Nicos Makris. March 2001.
- PEER 2001/01** *Experimental Study of Large Seismic Steel Beam-to-Column Connections.* Egor P. Popov and Shakhzod M. Takhirov. November 2000.
- PEER 2000/10** *The Second U.S.-Japan Workshop on Performance-Based Earthquake Engineering Methodology for Reinforced Concrete Building Structures.* March 2000.
- PEER 2000/09** *Structural Engineering Reconnaissance of the August 17, 1999 Earthquake: Kocaeli (Izmit), Turkey.* Halil Sezen, Kenneth J. Elwood, Andrew S. Whittaker, Khalid Mosalam, John J. Wallace, and John F. Stanton. December 2000.
- PEER 2000/08** *Behavior of Reinforced Concrete Bridge Columns Having Varying Aspect Ratios and Varying Lengths of Confinement.* Anthony J. Calderone, Dawn E. Lehman, and Jack P. Moehle. January 2001.
- PEER 2000/07** *Cover-Plate and Flange-Plate Reinforced Steel Moment-Resisting Connections.* Taejin Kim, Andrew S. Whittaker, Amir S. Gilani, Vitelmo V. Bertero, and Shakhzod M. Takhirov. September 2000.
- PEER 2000/06** *Seismic Evaluation and Analysis of 230-kV Disconnect Switches.* Amir S. J. Gilani, Andrew S. Whittaker, Gregory L. Fenves, Chun-Hao Chen, Henry Ho, and Eric Fujisaki. July 2000.
- PEER 2000/05** *Performance-Based Evaluation of Exterior Reinforced Concrete Building Joints for Seismic Excitation.* Chandra Clyde, Chris P. Pantelides, and Lawrence D. Reaveley. July 2000.
- PEER 2000/04** *An Evaluation of Seismic Energy Demand: An Attenuation Approach.* Chung-Che Chou and Chia-Ming Uang. July 1999.
- PEER 2000/03** *Framing Earthquake Retrofitting Decisions: The Case of Hillside Homes in Los Angeles.* Detlof von Winterfeldt, Neils Roselund, and Alicia Kitsuse. March 2000.
- PEER 2000/02** *U.S.-Japan Workshop on the Effects of Near-Field Earthquake Shaking.* Andrew Whittaker, Editor. July 2000.
- PEER 2000/01** *Further Studies on Seismic Interaction in Interconnected Electrical Substation Equipment.* Armen Der Kiureghian, Kee-Jeung Hong, and Jerome L. Sackman. November 1999.
- PEER 1999/14** *Seismic Evaluation and Retrofit of 230-kV Porcelain Transformer Bushings.* Amir S. Gilani, Andrew S. Whittaker, Gregory L. Fenves, and Eric Fujisaki. December 1999.
- PEER 1999/13** *Building Vulnerability Studies: Modeling and Evaluation of Tilt-up and Steel Reinforced Concrete Buildings.* John W. Wallace, Jonathan P. Stewart, and Andrew S. Whittaker, Editors. December 1999.
- PEER 1999/12** *Rehabilitation of Nonductile RC Frame Building Using Encasement Plates and Energy-Dissipating Devices.* Mehrdad Sasani, Vitelmo V. Bertero, James C. Anderson. December 1999.
- PEER 1999/11** *Performance Evaluation Database for Concrete Bridge Components and Systems under Simulated Seismic Loads.* Yael D. Hose and Frieder Seible. November 1999.
- PEER 1999/10** *U.S.-Japan Workshop on Performance-Based Earthquake Engineering Methodology for Reinforced Concrete Building Structures.* December 1999.
- PEER 1999/09** *Performance Improvement of Long Period Building Structures Subjected to Severe Pulse-Type Ground Motions.* James C. Anderson, Vitelmo V. Bertero, and Raul Bertero. October 1999.
- PEER 1999/08** *Envelopes for Seismic Response Vectors.* Charles Menun and Armen Der Kiureghian. July 1999.
- PEER 1999/07** *Documentation of Strengths and Weaknesses of Current Computer Analysis Methods for Seismic Performance of Reinforced Concrete Members.* William F. Cofer. November 1999.
- PEER 1999/06** *Rocking Response and Overturning of Anchored Equipment under Seismic Excitations.* Nicos Makris and Jian Zhang. November 1999.
- PEER 1999/05** *Seismic Evaluation of 550 kV Porcelain Transformer Bushings.* Amir S. Gilani, Andrew S. Whittaker, Gregory L. Fenves, and Eric Fujisaki. October 1999.
- PEER 1999/04** *Adoption and Enforcement of Earthquake Risk-Reduction Measures.* Peter J. May, Raymond J. Burby, T. Jens Feeley, and Robert Wood. August 1999.
- PEER 1999/03** *Task 3 Characterization of Site Response General Site Categories.* Adrian Rodriguez-Marek, Jonathan D. Bray and Norman Abrahamson. February 1999.
- PEER 1999/02** *Capacity-Demand-Diagram Methods for Estimating Seismic Deformation of Inelastic Structures: SDF Systems.* Anil K. Chopra and Rakesh Goel. April 1999.

- PEER 1999/01** *Interaction in Interconnected Electrical Substation Equipment Subjected to Earthquake Ground Motions.* Armen Der Kiureghian, Jerome L. Sackman, and Kee-Jeung Hong. February 1999.
- PEER 1998/08** *Behavior and Failure Analysis of a Multiple-Frame Highway Bridge in the 1994 Northridge Earthquake.* Gregory L. Fenves and Michael Ellery. December 1998.
- PEER 1998/07** *Empirical Evaluation of Inertial Soil-Structure Interaction Effects.* Jonathan P. Stewart, Raymond B. Seed, and Gregory L. Fenves. November 1998.
- PEER 1998/06** *Effect of Damping Mechanisms on the Response of Seismic Isolated Structures.* Nicos Makris and Shih-Po Chang. November 1998.
- PEER 1998/05** *Rocking Response and Overturning of Equipment under Horizontal Pulse-Type Motions.* Nicos Makris and Yiannis Roussos. October 1998.
- PEER 1998/04** *Pacific Earthquake Engineering Research Invitational Workshop Proceedings, May 14–15, 1998: Defining the Links between Planning, Policy Analysis, Economics and Earthquake Engineering.* Mary Comerio and Peter Gordon. September 1998.
- PEER 1998/03** *Repair/Upgrade Procedures for Welded Beam to Column Connections.* James C. Anderson and Xiaojing Duan. May 1998.
- PEER 1998/02** *Seismic Evaluation of 196 kV Porcelain Transformer Bushings.* Amir S. Gilani, Juan W. Chavez, Gregory L. Fenves, and Andrew S. Whittaker. May 1998.
- PEER 1998/01** *Seismic Performance of Well-Confining Concrete Bridge Columns.* Dawn E. Lehman and Jack P. Moehle. December 2000.

PEER REPORTS: ONE HUNDRED SERIES

The following PEER reports are available by Internet only at http://peer.berkeley.edu/publications/peer_reports_complete.html.

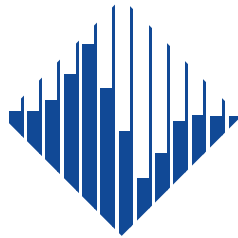
- PEER 2012/103** *Performance-Based Seismic Demand Assessment of Concentrically Braced Steel Frame Buildings.* Chui-Hsin Chen and Stephen A. Mahin. December 2012.
- PEER 2012/102** *Procedure to Restart an Interrupted Hybrid Simulation: Addendum to PEER Report 2010/103.* Vesna Terzic and Božidar Stojadinovic. October 2012.
- PEER 2012/101** *Mechanics of Fiber Reinforced Bearings.* James M. Kelly and Andrea Calabrese. February 2012.
- PEER 2011/107** *Nonlinear Site Response and Seismic Compression at Vertical Array Strongly Shaken by 2007 Niigata-ken Chuetsu-oki Earthquake.* Eric Yee, Jonathan P. Stewart, and Kohji Tokimatsu. December 2011.
- PEER 2011/106** *Self Compacting Hybrid Fiber Reinforced Concrete Composites for Bridge Columns.* Pardeep Kumar, Gabriel Jen, William Trono, Marios Panagiotou, and Claudia Osterdag. September 2011.
- PEER 2011/105** *Stochastic Dynamic Analysis of Bridges Subjected to Spatially Varying Ground Motions.* Katerina Konakli and Armen Der Kiureghian. August 2011.
- PEER 2011/104** *Design and Instrumentation of the 2010 E-Defense Four-Story Reinforced Concrete and Post-Tensioned Concrete Buildings.* Takuya Nagae, Kenichi Tahara, Taizo Matsumori, Hitoshi Shiohara, Toshimi Kabeyasawa, Susumu Kono, Minehiro Nishiyama (Japanese Research Team) and John Wallace, Wassim Ghannoum, Jack Moehle, Richard Sause, Wesley Keller, Zeynep Tuna (U.S. Research Team). June 2011.
- PEER 2011/103** *In-Situ Monitoring of the Force Output of Fluid Dampers: Experimental Investigation.* Dimitrios Konstantinidis, James M. Kelly, and Nicos Makris. April 2011.
- PEER 2011/102** *Ground-Motion Prediction Equations 1964–2010.* John Douglas. April 2011.
- PEER 2011/101** *Report of the Eighth Planning Meeting of NEES/E-Defense Collaborative Research on Earthquake Engineering.* Convened by the Hyogo Earthquake Engineering Research Center (NIED), NEES Consortium, Inc. February 2011.
- PEER 2010/111** *Modeling and Acceptance Criteria for Seismic Design and Analysis of Tall Buildings.* Task 7 Report for the Tall Buildings Initiative - Published jointly by the Applied Technology Council. October 2010.
- PEER 2010/110** *Seismic Performance Assessment and Probabilistic Repair Cost Analysis of Precast Concrete Cladding Systems for Multistory Buildings.* Jeffrey P. Hunt and Božidar Stojadinovic. November 2010.
- PEER 2010/109** *Report of the Seventh Joint Planning Meeting of NEES/E-Defense Collaboration on Earthquake Engineering. Held at the E-Defense, Miki, and Shin-Kobe, Japan, September 18–19, 2009.* August 2010.
- PEER 2010/108** *Probabilistic Tsunami Hazard in California.* Hong Kie Thio, Paul Somerville, and Jascha Polet, preparers. October 2010.
- PEER 2010/107** *Performance and Reliability of Exposed Column Base Plate Connections for Steel Moment-Resisting Frames.* Ady Aviram, Božidar Stojadinovic, and Armen Der Kiureghian. August 2010.
- PEER 2010/106** *Verification of Probabilistic Seismic Hazard Analysis Computer Programs.* Patricia Thomas, Ivan Wong, and Norman Abrahamson. May 2010.
- PEER 2010/105** *Structural Engineering Reconnaissance of the April 6, 2009, Abruzzo, Italy, Earthquake, and Lessons Learned.* M. Selim Günay and Khalid M. Mosalam. April 2010.
- PEER 2010/104** *Simulating the Inelastic Seismic Behavior of Steel Braced Frames, Including the Effects of Low-Cycle Fatigue.* Yuli Huang and Stephen A. Mahin. April 2010.
- PEER 2010/103** *Post-Earthquake Traffic Capacity of Modern Bridges in California.* Vesna Terzic and Božidar Stojadinović. March 2010.
- PEER 2010/102** *Analysis of Cumulative Absolute Velocity (CAV) and JMA Instrumental Seismic Intensity (I_{JMA}) Using the PEER-NGA Strong Motion Database.* Kenneth W. Campbell and Yousef Bozorgnia. February 2010.
- PEER 2010/101** *Rocking Response of Bridges on Shallow Foundations.* Jose A. Ugalde, Bruce L. Kutter, and Boris Jeremic. April 2010.
- PEER 2009/109** *Simulation and Performance-Based Earthquake Engineering Assessment of Self-Centering Post-Tensioned Concrete Bridge Systems.* Won K. Lee and Sarah L. Billington. December 2009.

- PEER 2009/108** *PEER Lifelines Geotechnical Virtual Data Center.* J. Carl Stepp, Daniel J. Ponti, Loren L. Turner, Jennifer N. Swift, Sean Devlin, Yang Zhu, Jean Benoit, and John Bobbitt. September 2009.
- PEER 2009/107** *Experimental and Computational Evaluation of Current and Innovative In-Span Hinge Details in Reinforced Concrete Box-Girder Bridges: Part 2: Post-Test Analysis and Design Recommendations.* Matias A. Hube and Khalid M. Mosalam. December 2009.
- PEER 2009/106** *Shear Strength Models of Exterior Beam-Column Joints without Transverse Reinforcement.* Sangjoon Park and Khalid M. Mosalam. November 2009.
- PEER 2009/105** *Reduced Uncertainty of Ground Motion Prediction Equations through Bayesian Variance Analysis.* Robb Eric S. Moss. November 2009.
- PEER 2009/104** *Advanced Implementation of Hybrid Simulation.* Andreas H. Schellenberg, Stephen A. Mahin, Gregory L. Fenves. November 2009.
- PEER 2009/103** *Performance Evaluation of Innovative Steel Braced Frames.* T. Y. Yang, Jack P. Moehle, and Božidar Stojadinovic. August 2009.
- PEER 2009/102** *Reinvestigation of Liquefaction and Nonliquefaction Case Histories from the 1976 Tangshan Earthquake.* Robb Eric Moss, Robert E. Kayen, Liyuan Tong, Songyu Liu, Guojun Cai, and Jiae Wu. August 2009.
- PEER 2009/101** *Report of the First Joint Planning Meeting for the Second Phase of NEES/E-Defense Collaborative Research on Earthquake Engineering.* Stephen A. Mahin et al. July 2009.
- PEER 2008/104** *Experimental and Analytical Study of the Seismic Performance of Retaining Structures.* Linda Al Atik and Nicholas Sitar. January 2009.
- PEER 2008/103** *Experimental and Computational Evaluation of Current and Innovative In-Span Hinge Details in Reinforced Concrete Box-Girder Bridges. Part 1: Experimental Findings and Pre-Test Analysis.* Matias A. Hube and Khalid M. Mosalam. January 2009.
- PEER 2008/102** *Modeling of Unreinforced Masonry Infill Walls Considering In-Plane and Out-of-Plane Interaction.* Stephen Kadysiewski and Khalid M. Mosalam. January 2009.
- PEER 2008/101** *Seismic Performance Objectives for Tall Buildings.* William T. Holmes, Charles Kircher, William Petak, and Nabih Youssef. August 2008.
- PEER 2007/101** *Generalized Hybrid Simulation Framework for Structural Systems Subjected to Seismic Loading.* Tarek Elkhoraibi and Khalid M. Mosalam. July 2007.
- PEER 2007/100** *Seismic Evaluation of Reinforced Concrete Buildings Including Effects of Masonry Infill Walls.* Alidad Hashemi and Khalid M. Mosalam. July 2007.

The Pacific Earthquake Engineering Research Center (PEER) is a multi-institutional research and education center with headquarters at the University of California, Berkeley. Investigators from over 20 universities, several consulting companies, and researchers at various state and federal government agencies contribute to research programs focused on performance-based earthquake engineering.

These research programs aim to identify and reduce the risks from major earthquakes to life safety and to the economy by including research in a wide variety of disciplines including structural and geotechnical engineering, geology/seismology, lifelines, transportation, architecture, economics, risk management, and public policy.

PEER is supported by federal, state, local, and regional agencies, together with industry partners.



PEER Core Institutions

University of California, Berkeley (Lead Institution)
California Institute of Technology
Oregon State University
Stanford University
University of California, Davis
University of California, Irvine
University of California, Los Angeles
University of California, San Diego
University of Nevada, Reno
University of Southern California
University of Washington

PEER reports can be ordered at <https://peer.berkeley.edu/peer-reports> or by contacting

Pacific Earthquake Engineering Research Center
University of California, Berkeley
325 Davis Hall, Mail Code 1792
Berkeley, CA 94720-1792
Tel: 510-642-3437
Email: peer_center@berkeley.edu

ISSN 1547-0587X